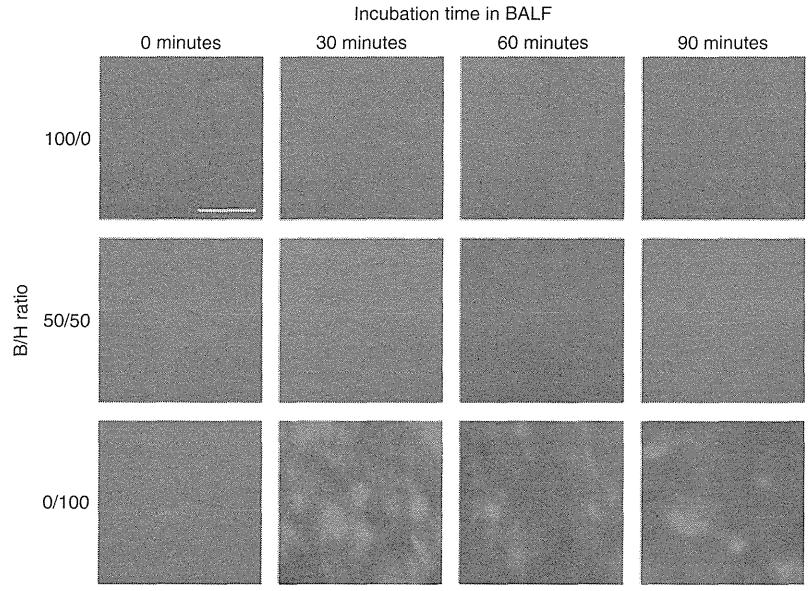

Figure 6 Aggregation of polyplexes during the incubation in bronchoalveolar lavage fluid (BALF). The polypexes were prepared from Cy5-labeled plasmid DNAs (pDNAs), and after adding BALF, the polyplex solutions were observed by a fluorescent microscope. Bar = 50 μm.

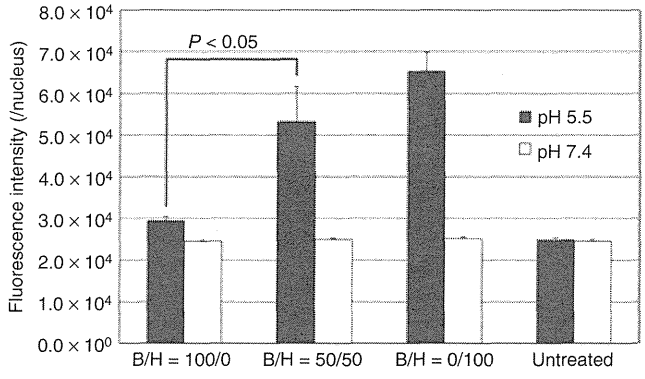

Figure 7 Evaluation of cell membrane destabilization at pH 5.5 or 7.4 in the culture medium. After 30 minutes of transfection toward HuH-7, cells were treated with YO-PRO1. The fluorescence intensity in each cell nucleus, indicating the amount of YO-PRO1 penetration through the plasma membrane, was determined using IN Cell Analyzer 1000. The averages from about 3,000 cells were analyzed in each well. The data were expressed as the means ± SEM (N = 5).

B/H = 0/100 formulation in the lung may elicit acute inflammatory responses, resulting in reduced transgene expressions. Notably, appropriate PEG shielding of the polyplex prevented aggregate formation effectively, and polyplexes with B/H = 50/50 formulation achieved appreciable gene expression in the lungs without inflammatory responses. Therefore, this polyplex formulation is a highly practical system for gene therapy for the respiratory system that takes advantage of both effective PEG shielding and functioning of PAsp(DET) polycations to enhance endosomal escape.

MATERIALS AND METHODS

Materials. PEG-block-PAsp(DET) block copolymer (B) and PAsp(DET) homo polymer (H) were synthesized as previously reported.[13] The PEG used in this study had a molecular weight of 12,000 Da. The degree of polymerization of PAsp(DET) portion for B and H was determined by ^{1}H-NMR analyses to be 60 and 55, respectively. CpG-depleted pDNA encoding luciferase (pCpG-ΔLuc) was kindly provided by Makiya Nishikawa from Kyoto University (Kyoto, Japan), which had been constructed as previously reported.[34] The pDNA was amplified in GT115 Escherichia coli (InvivoGen, San Diego, CA) and purified using NucleoBond Xtra EF (Nippon Genetics, Tokyo, Japan). The pDNA concentration was determined spectroscopically at 260 nm. Dulbecco's modified Eagle's medium and fetal bovine serum were purchased from Sigma–Aldrich (St Louis, MO) and Life Technologies Japan (Tokyo, Japan), respectively. Linear polyethylenimine (Exgen 500, molecular weight = 22 kDa) was purchased from MBI FerMentas (Burlington, Ontario, Canada).

Preparation of polyplex solutions. Each polyplex sample was prepared by mixing pDNA and polycations B and/or H at the indicated ratio. The N/P ratio [(total amines in polycations)]/(DNA phosphates)] was fixed at eight throughout the study.

In vitro transfection. Mouse embryonic fibroblast and hepatocellular carcinoma (HuH-7) cells were seeded at a density of 5,000 cells/well in 96-well culture plates and incubated overnight in 100 ml Dulbecco's modified Eagle's medium supplemented with 10% fetal bovine serum and penicillin/streptomycin. For each transfection, the culture medium was replaced with fresh medium containing 10% fetal bovine serum, and the polyplex solution containing 0.25 μg of pDNA was administered to each well. Luciferase expression was measured with the Luciferase assay system (Promega, Madison, WI) and the GloMaxTM 96 microplate luminometer (Promega) according to the manufacturer's protocol.

Intratracheal gene introduction into mouse lungs. BALB/c mice (female, 7 weeks old) were purchased from Charles River Laboratories (Yokohama, Japan). Mice were anesthetized intraperitoneally with pentobarbital (60 mg/kg) (Kyoritsu Seiyaku, Tokyo, Japan). Fifty microliter of polyplex solution containing 10 μg pDNA was administered using a microsprayer model IA-1C-R (Penn Century, Philadelphia, PA) after tracheostomies. All animal protocols were conducted with the approval of the Animal Care and Use Committee, University of Tokyo, Tokyo, Japan.

Evaluation of luciferase expressions in lung. Mice were sacrificed after 24 hours, and lung was excised and thoroughly homogenized using a Multibeads shocker (Yasui Kikai, Osaka, Japan). Luciferase expression was

measured by a luciferase assay system using the Lumat LB9507 luminometer (Berthold, Bad Wildbad, Germany). The expression was normalized to protein concentrations in the cell lysates.

Histological evaluations. Lung specimens were fixed in 10% formalin for 24 hours and embedded in paraffin. These sections (5-μm thick) were stained with hematoxylin and eosin. For evaluations of polyplex behavior and macrophages, pDNA was labeled with Cy-5 using Label IT Tracker Intracellular Nucleic Acid Localization Kits (Mirus, Madison, WI) following manufacturer's protocol. Mice were sacrificed after 4 hours and the excised lung tissue was fixed in 10% formalin for 5 hours, followed by overnight incubation in 20% sucrose/phosphate-buffered saline (PBS) solution at room temperature. The specimens were frozen and sectioned at a 10-μm thickness in a cryostat. Macrophages were immunostained with an anti-F4/80 monoclonal antibody (AbD Serotec, Oxford, UK) at a dilution of 1:300 and an Alexa488-conjugated secondary antibody (Invitrogen, Carlsbad, CA). After staining the nuclei with Hoechst 33342 (Dojindo, Kumamoto, Japan), the sections were observed with a fluorescence microscope equipped with image-analysis software (IN Cell Analyzer 1000; GE Healthcare UK), followed by the measurement of fluorescence intensity of Cy-5 labeled DNA in each macrophage. About 300 macrophages were analyzed for each group.

Measurement of proinflammatory cytokines. To measure mRNA levels of proinflammatory cytokines (IL-6, tumor necrosis factor-α, and IL-10) and cyclooxygenase-2, lung tissue was extracted and total RNA was isolated using an RNeasy Mini Preparation Kit (Qiagen, Hilden, Germany) following manufacturer's protocol. Gene expressions were analyzed by real-time quantitative PCR using TaqMan Gene Expression Assays (Mm00446190_m1 for IL-6, Mm00443258 for tumor necrosis factor-α, Mm 01288386_m1 for IL-10, Mm01307334_g1 for cyclooxygenase-2, and Mm00607939 for β-actin) and an ABI Prism 7500 Sequence Detector (Applied Biosystems, Foster City, CA).

Observation of aggregation in BALF. BAL was performed with 500 μl PBS (instilled and recovered four times), and the BAL fluid (BALF) obtained was centrifuged at 300*g*. To observe the aggregation of polyplexes, Cy5-labeled DNA was used to prepare polyplex solutions at DNA concentration of 33.3 μg/ml. BALF was added to equal volumes of polyplex solutions and observed with an Axiovert 200 fluorescence microscope (Carl Zeiss, Jena, Germany) using a 20× EC Plan Neofuar objective (Carl Zeiss).

Measurement of cellular uptake in lung cells. BAL was conducted eight times, using 500 μl PBS in each time, to remove extracellular pDNA. Next, pDNA was collected from the excised lung tissue and purified using a Wizard Genomic DNA Purification Kit (Promega). Purified DNA was then subjected to a real-time PCR to quantify pDNA copies using an ABI Prism 7500 Sequence Detector (Applied Biosystems). The forward primer (TCTGTGGCTTCAGAGTGGTG) and reverse primer (CTGATTCCTGGGAGATGGAA) were used because they are specific for pCpG-ΔLuc. The copy number of β-actin was also determined by TaqMan Gene Expression Assays to normalize the cell number.

Evaluation of endosomal escape inside cells. HuH-7 cells were seeded at a density of 10,000 cells/well in a 48-multiwell plate and cultured for 24 hours. The culture medium was then replaced with PBS buffer (pH 7.4) or MES buffer (pH 5.5) containing 20 mmol/l MES and 150 mmol/l NaCl; a polyplex solution containing 0.5 μg pDNA was added to each well. The cells were treated with 1 μmol/l YO-PRO1 (Invitrogen) and 2.5 μg/ml Hoechst 33342 in PBS 30 minutes later. The fluorescence intensity of each nucleus was quantified after a 10-minute incubation using an IN Cell Analyzer 1000.

SUPPLEMENTARY MATERIAL

Figure S1 . Messenger RNA expression of proinflammatory cytokines and Cox-2 in lung at 4 hours and 24 hours after transfection.

Figure S2. Blood tests at 24 hours after administration.

Figure S3. Uptake of polyplexes by lung cells at 24 hours after transfection.

ACKNOWLEDGMENTS

We deeply appreciate Makiya Nishikawa (Kyoto University) for providing pDNA (pCpG-ΔLuc), and E.S. (National Cerebral and Cardiovascular Center Research Institute) for technical advices on lung administration of polyplexes. This work was financially supported in part by the Core Research Program for Evolutional Science and Technology (CREST) from Japan Science and Technology Corporation (JST) (K.K.), Grants-in-Aid for Scientific Research form the Japanese Ministry of Education, Culture, Sports, Science and Technology, Japan (MEXT) (K.I.), Global COE Program "Medical System Innovation on through Multidisciplinary Integration" from MEXT, Japan, and Funding Program for World-Leading Innovative R&D on Science and Technology (FIRST Program) from the Japan Society for the Promotion of Science (JSPS). We also thank Satomi Ogura, Yoko Hasegawa, and Katsue Morii (The University of Tokyo) for technical assistance.

REFERENCES

1. Howell, TH, Fiorellini, J, Jones, A, Alder, M, Nummikoski, P, Lazaro, M *et al.* (1997). A feasibility study evaluating rhBMP-2/absorbable collagen sponge device for local alveolar ridge preservation or augmentation. *Int J Periodontics Restorative Dent* **17**: 124–139.
2. Sanders, N, Rudolph, C, Braeckmans, K, De Smedt, SC and Demeester, J (2009). Extracellular barriers in respiratory gene therapy. *Adv Drug Deliv Rev* **61**: 115–127.
3. Oupický, D, Konák, C, Ulbrich, K, Wolfert, MA and Seymour, LW (2000). DNA delivery systems based on complexes of DNA with synthetic polycations and their copolymers. *J Control Release* **65**: 149–171.
4. Kakizawa, Y and Kataoka, K (2002). Block copolymer micelles for delivery of gene and related compounds. *Adv Drug Deliv Rev* **54**: 203–222.
5. De Smedt, SC, Demeester, J and Hennink, WE (2000). Cationic polymer based gene delivery systems. *Pharm Res* **17**: 113–126.
6. Nel, A, Xia, T, Mädler, L and Li, N (2006). Toxic potential of materials at the nanolevel. *Science* **311**: 622–627.
7. Card, JW, Zeldin, DC, Bonner, JC and Nestmann, ER (2008). Pulmonary applications and toxicity of engineered nanoparticles. *Am J Physiol Lung Cell Mol Physiol* **295**: L400–L411.
8. Bonner, JC (2010). Nanoparticles as a potential cause of pleural and interstitial lung disease. *Proc Am Thorac Soc* **7**: 138–141.
9. Poland, CA, Duffin, R, Kinloch, I, Maynard, A, Wallace, WA, Seaton, A *et al.* (2008). Carbon nanotubes introduced into the abdominal cavity of mice show asbestos-like pathogenicity in a pilot study. *Nat Nanotechnol* **3**: 423–428.
10. Ryman-Rasmussen, JP, Cesta, MF, Brody, AR, Shipley-Phillips, JK, Everitt, JI, Tewksbury, EW *et al.* (2009). Inhaled carbon nanotubes reach the subpleural tissue in mice. *Nat Nanotechnol* **4**: 747–751.
11. Beyerle, A, Irmler, M, Beckers, J, Kissel, T and Stoeger, T (2010). Toxicity pathway focused gene expression profiling of PEI-based polymers for pulmonary applications. *Mol Pharm* **7**: 727–737.
12. Dailey, LA, Jekel, N, Fink, L, Gessler, T, Schmehl, T, Wittmar, M *et al.* (2006). Investigation of the proinflammatory potential of biodegradable nanoparticle drug delivery systems in the lung. *Toxicol Appl Pharmacol* **215**: 100–108.
13. Kanayama, N, Fukushima, S, Nishiyama, N, Itaka, K, Jang, WD, Miyata, K *et al.* (2006). A PEG-based biocompatible block catiomer with high buffering capacity for the construction of polyplex micelles showing efficient gene transfer toward primary cells. *ChemMedChem* **1**: 439–444.
14. Masago, K, Itaka, K, Nishiyama, N, Chung, UI and Kataoka, K (2007). Gene delivery with biocompatible cationic polymer: pharmacogenomic analysis on cell bioactivity. *Biomaterials* **28**: 5169–5175.
15. Harada-Shiba, M, Takamisawa, I, Miyata, K, Ishii, T, Nishiyama, N, Itaka, K *et al.* (2009). Intratracheal gene transfer of adrenomedullin using polyplex nanomicelles attenuates monocrotaline-induced pulmonary hypertension in rats. *Mol Ther* **17**: 1180–1186.
16. Miyata, K, Oba, M, Nakanishi, M, Fukushima, S, Yamasaki, Y, Koyama, H *et al.* (2008). Polyplexes from poly(aspartamide) bearing 1,2-diaminoethane side chains induce pH-selective, endosomal membrane destabilization with amplified transfection and negligible cytotoxicity. *J Am Chem Soc* **130**: 16287–16294.
17. Itaka, K, Ishii, T, Hasegawa, Y and Kataoka, K (2010). Biodegradable polyamino acid-based polycations as safe and effective gene carrier minimizing cumulative toxicity. *Biomaterials* **31**: 3707–3714.
18. Maruyama, K, Yuda, T, Okamoto, A, Kojima, S, Suginaka, A and Iwatsuru, M (1992). Prolonged circulation time *in vivo* of large unilamellar liposomes composed of distearoyl phosphatidylcholine and cholesterol containing amphipathic poly(ethylene glycol). *Biochim Biophys Acta* **1128**: 44–49.
19. Ogris, M, Brunner, S, Schüller, S, Kircheis, R and Wagner, E (1999). PEGylated DNA/transferrin-PEI complexes: reduced interaction with blood components, extended circulation in blood and potential for systemic gene delivery. *Gene Ther* **6**: 595–605.
20. Verbaan, FJ, Oussoren, C, Snel, CJ, Crommelin, DJ, Hennink, WE and Storm, G (2004). Steric stabilization of poly(2-(dimethylamino)ethyl methacrylate)-based polyplexes mediates prolonged circulation and tumor targeting in mice. *J Gene Med* **6**: 64–75.

21. Itaka, K and Kataoka, K (2009). Recent development of nonviral gene delivery systems with virus-like structures and mechanisms. *Eur J Pharm Biopharm* **71**: 475–483.
22. Kursa, M, Walker, GF, Roessler, V, Ogris, M, Roedl, W, Kircheis, R *et al.* (2003). Novel shielded transferrin-polyethylene glycol-polyethylenimine/DNA complexes for systemic tumor-targeted gene transfer. *Bioconjug Chem* **14**: 222–231.
23. Allen, TM, Mehra, T, Hansen, C and Chin, YC (1992). Stealth liposomes: an improved sustained release system for 1-beta-D-arabinofuranosylcytosine. *Cancer Res* **52**: 2431–2439.
24. Itaka, K, Ohba, S, Miyata, K, Kawaguchi, H, Nakamura, K, Takato, T *et al.* (2007). Bone regeneration by regulated *in vivo* gene transfer using biocompatible polyplex nanomicelles. *Mol Ther* **15**: 1655–1662.
25. Akagi, D, Oba, M, Koyama, H, Nishiyama, N, Fukushima, S, Miyata, T *et al.* (2007). Biocompatible micellar nanovectors achieve efficient gene transfer to vascular lesions without cytotoxicity and thrombus formation. *Gene Ther* **14**: 1029–1038.
26. Sagara, K and Kim, SW (2002). A new synthesis of galactose-poly(ethylene glycol)-polyethylenimine for gene delivery to hepatocytes. *J Control Release* **79**: 271–281.
27. Brissault, B, Kichler, A, Leborgne, C, Danos, O, Cheradame, H, Gau, J *et al.* (2006). Synthesis, characterization, and gene transfer application of poly(ethylene glycol-b-ethylenimine) with high molar mass polyamine block. *Biomacromolecules* **7**: 2863–2870.
28. Tabata, Y and Ikada, Y (1988). Effect of the size and surface charge of polymer microspheres on their phagocytosis by macrophage. *Biomaterials* **9**: 356–362.
29. Midoux, P, Mayer, R and Monsigny, M (1995). Membrane permeabilization by alpha-helical peptides: a flow cytometry study. *Biochim Biophys Acta* **1239**: 249–256.
30. Uchida, S, Itaka, K, Chen, Q, Osada, K, Miyata, K, Ishii, T *et al.* (2011). Combination of chondroitin sulfate and polyplex micelles from Poly(ethylene glycol)-poly{N'-[N-(2-aminoethyl)-2-aminoethyl]aspartamide} block copolymer for prolonged *in vivo* gene transfection with reduced toxicity. *J Control Release* **155**: 296–302.
31. Vernier, PT, Sun, Y and Gundersen, MA (2006). Nanoelectropulse-driven membrane perturbation and small molecule permeabilization. *BMC Cell Biol* **7**: 37.
32. Beyerle, A, Merkel, O, Stoeger, T and Kissel, T (2010). PEGylation affects cytotoxicity and cell-compatibility of poly(ethylene imine) for lung application: structure-function relationships. *Toxicol Appl Pharmacol* **242**: 146–154.
33. Takae, S, Miyata, K, Oba, M, Ishii, T, Nishiyama, N, Itaka, K *et al.* (2008). PEG-detachable polyplex micelles based on disulfide-linked block catiomers as bioresponsive nonviral gene vectors. *J Am Chem Soc* **130**: 6001–6009.
34. Mitsui, M, Nishikawa, M, Zang, L, Ando, M, Hattori, K, Takahashi, Y *et al.* (2009). Effect of the content of unmethylated CpG dinucleotides in plasmid DNA on the sustainability of transgene expression. *J Gene Med* **11**: 435–443.

PLOS ONE

In Vivo Messenger RNA Introduction into the Central Nervous System Using Polyplex Nanomicelle

Satoshi Uchida[1], Keiji Itaka[1]*, Hirokuni Uchida[2], Kentaro Hayakawa[3], Toru Ogata[3], Takehiko Ishii[2], Shigeto Fukushima[4], Kensuke Osada[4], Kazunori Kataoka[1,2,4]*

1 Division of Clinical Biotechnology, Center for Disease Biology and Integrative Medicine, Graduate School of Medicine, The University of Tokyo, Bunkyo-ku, Tokyo, Japan, **2** Department of Bioengineering, Graduate School of Engineering, The University of Tokyo, Bunkyo-ku, Tokyo, Japan, **3** Department of Rehabilitation for the Movement Functions, Research Institute, National Rehabilitation Center for the Persons With Disabilities, Tokorozawa, Saitama, Japan, **4** Department of Materials Engineering, Graduate School of Engineering, The University of Tokyo, Bunkyo-ku, Tokyo, Japan

Abstract

Messenger RNA (mRNA) introduction is a promising approach to produce therapeutic proteins and peptides without any risk of insertion mutagenesis into the host genome. However, it is difficult to introduce mRNA *in vivo* mainly because of the instability of mRNA under physiological conditions and its strong immunogenicity through the recognition by Toll-like receptors (TLRs). We used a novel carrier based on self-assembly of a polyethylene glycol (PEG)-polyamino acid block copolymer, polyplex nanomicelle, to administer mRNA into the central nervous system (CNS). The nanomicelle with 50 nm in diameter has a core-shell structure with mRNA-containing inner core surrounded by PEG layer, providing the high stability and stealth property to the nanomicelle. The functional polyamino acids possessing the capacity of pH-responsive membrane destabilization allows smooth endosomal escape of the nanomicelle into the cytoplasm. After introduction into CNS, the nanomicelle successfully provided the sustained protein expression in the cerebrospinal fluid for almost a week. Immune responses after mRNA administration into CNS were effectively suppressed by the use of the nanomicelle compared with naked mRNA introduction. *In vitro* analyses using specific TLR-expressing HEK293 cells confirmed that the nanomicelle inclusion prevented mRNA from the recognition by TLRs. Thus, the polyplex nanomicelle is a promising system that simultaneously resolved the two major problems of *in vivo* mRNA introduction, the instability and immunogenicity, opening the door to various new therapeutic strategies using mRNA.

Citation: Uchida S, Itaka K, Uchida H, Hayakawa K, Ogata T, et al. (2013) *In Vivo* Messenger RNA Introduction into the Central Nervous System Using Polyplex Nanomicelle. PLoS ONE 8(2): e56220. doi:10.1371/journal.pone.0056220

Editor: Maria Gasset, Consejo Superior de Investigaciones Cientificas, Spain

Received September 26, 2012; **Accepted** January 7, 2013; **Published** February 13, 2013

Funding: This work was financially supported in part by the Core Research Program for Evolutional Science and Technology (CREST) from Japan Science and Technology Corporation (JST) (K.K., http://www.jst.go.jp/kisoken/crest/en/index.html), Grants-in-Aid for Scientific Research form the Japanese Ministry of Education, Culture, Sports, Science and Technology, Japan (MEXT) (K.I., http://www.jsps.go.jp/english/e-grants/index.html), Global COE Program 'Medical System Innovation through Multidisciplinary Integration' from MEXT, Japan (http://park.itc.u-tokyo.ac.jp/CMSI/e/index.html) and Funding Program for World-Leading Innovative R&D on Science and Technology (FIRST Program) from the Japan Society for the Promotion of Science (JSPS) (http://www.jsps.go.jp/english/index.html). The funders had no role in study design, data collection and analysis, decision to publish, or preparation of the manuscript.

Competing Interests: The authors have declared that no competing interests exist.

* E-mail: itaka-ort@umin.net (KI); kataoka@bmw.t.u-tokyo.ac.jp (KK)

Introduction

Messenger RNA (mRNA) has a high potential to produce proteins or peptides for therapeutic purposes in a safe manner without any risk of random integration into the genome. Although pioneering studies to transfect mRNA into cells using a nonviral method were reported in the 1980s [1,2], the interest in the clinical use of mRNA has been limited for a long time. There are two major problems associated with mRNA introduction: mRNA is considered to be unstable to obtain sufficient protein expression in clinical settings [3] and mRNA induces strong immune reactions through recognition by Toll-like receptors (TLRs) [4,5], hampering repeated mRNA administration. Thus, efforts for clinical applications of mRNA have been limited, mainly in cancer immunotherapy by *ex vivo* transfection toward dendritic cells [6,7,8,9]. In contrast, there are only a few studies reporting the trials of *in vivo* mRNA administration [10,11].

Instability is an inherent limitation of mRNA. Many *in vitro* transfection studies have revealed that although mRNA enabled even higher efficiency of protein expression than plasmid DNA (pDNA) within several hours after mRNA introduction into cells, the duration of expression was apt to be very short [12,13]. For example, several groups recently induced pluripotent stem cells (iPSCs) by transfection of mRNA encoding Yamanaka factors [14,15,16]. Their success strongly suggests the feasibility of using mRNA for therapeutic purposes in the future; however, they generally performed repeat transfections with intervals of a few days, suggesting that the instability of mRNA hampered the durable protein expression after mRNA transfection.

Thus, the requirement of an effective mRNA delivery system to overcome the instability of mRNA should be further explored to realise *in vivo* mRNA administration. Although some strategies have been reported for nonviral *in vivo* mRNA administration, including injection of naked mRNA [17,18] in combination with physical pressure such as electroporation or gene gun [1,19] and the usage of synthetic carriers based on cationic lipids and polymers [20,21,22], low efficiency and short duration of protein expression remain significant problems to be solved. At present,

there is only one phase 1 study clinical trial to treat metastatic melanoma by subcutaneous injection of naked or protamine-stabilised mRNAs [9]; however, a more efficient system for *in vivo* mRNA administration would be strongly required to expand the application to many other clinical fields.

In addition to the stability issue, the problem of mRNA immunogenicity also remains unsolved. Based on findings that mRNA containing modified nucleosides effectively suppresses recognition by TLRs [23,24], mRNA modification was proposed as an effective method to reduce immunogenicity. Several protocols for mRNA modification have been reported to effectively regulate the induction of inflammatory cytokines after mRNA administration, for example, replacement of uridine with pseudouridine [11,25] or replacement of 25% uridine and cytidine with 2-thiouridine and 5-methyl-cytidine [10]. However, cytokine induction was not completely eliminated even when using modified mRNA. Moreover, the modified forms of pseudouridine and thiouridine are rarely found in endogenous mRNA [26], leaving their clinical safety and availability unclear.

These issues motivated us to apply a new methodology using our original nonviral carrier, polyplex nanomicelle [27], for *in vivo* mRNA administration. As a result of its characteristic core–shell architecture based on the self assembly of block copolymers composed of polyethylene glycol (PEG) and polyamino acids, the polyplex nanomicelle has a strong potential to function as an effective mRNA-containing carrier with high stability and stealth properties, thereby simultaneously addressing the issues of instability and immunogenicity of mRNA.

To evaluate polyplex nanomicelle capacity, the central nervous system (CNS) was targeted. For treatments of chronic neurogenic disorders and spinal cord injuries, continuous administration of therapeutic proteins and peptides into the intrathecal space has many potential applications. The proteins and peptides are able to move along perivascular spaces and axon tracts into the spinal cord, avoiding the blood–brain barrier (BBB), the major obstacle to therapeutic delivery into CNS [28]. However, continuous delivery of proteins and peptides generally requires physical means such as indwelling catheters, which often involve many risks and complications. Secreted transgene products from either pDNA or mRNA that are introduced into the neural tissues are promising alternatives. In particular, mRNA is a strong candidate because there is no risk of random integration.

In this study, we applied the polyplex nanomicelle system using a polycation, poly[N′-[N-(2-aminoethyl)-2-aminoethyl]aspartamide] ([PAsp(DET)]), for mRNA administration into CNS [29,30,31]. The system was discovered to have a high capacity for enhanced endosomal escape because of pH-responsive membrane destabilization by [PAsp(DET)] [32] as well as the unique character of rapidly degrading into nontoxic forms under physiological conditions, thereby minimizing cell damage and toxicity that incidentally occur after introduction in a time-dependent manner [33,34]. By intrathecal injection into CNS, the feasibility of using the nanomicelle for *in vivo* mRNA administration was investigated through comprehensive analyses of continuous protein expression and regulated immunogenicity.

Results

Polyplex nanomicelle allowed *in vivo* mRNA introduction into CNS

First, luciferase-expressing mRNA with nucleoside modification was introduced into CNS using various carriers by intrathecal injection into the cisterna magna of mice. Luciferase expression was evaluated from extracts of the brain stem and surrounding neural tissue. Among the carriers, the polyplex nanomicelle with 50 nm in diameter (Fig. S1) composed of PEG–PAsp(DET) showed significantly higher luciferase expression than any other carriers including lipoplex (Lipofectamine 2000) and polyplexes without PEG shielding (Fig. 1). Luciferase expression by the nanomicelle was detected as early as 4 h after introduction and lasted for more than 24 h. Concomitantly, immunohistological analysis of CNS after introducing green fluorescent protein (GFP)-expressing mRNA using the polyplex nanomicelle revealed strong protein expression in meninges flanking the subarachnoid space (Fig. 2). We also analysed luciferase expression in other CNS sites away from the injection site of the occipital region. The expression was clearly detected from the brain to the lumbar region, strongly suggesting that the nanomicelle was widely distributed through the subarachnoid space (Fig. S2).

Polyplex nanomicelle effectively regulated the immunogenicity of mRNA

As mentioned in the Introduction, the immunogenicity of mRNA is a critical issue to achieve its effective and practical delivery into the body. This issue was addressed by analysing immune responses, including the induction of proinflammatory cytokines and type 1 interferon in CNS, after intrathecal injection of mRNA (modified or unmodified) in the form of naked mRNA or using the polyplex nanomicelle. Measurement of cytokines and type 1 interferons by quantitative polymerase chain reaction (qPCR) of total mRNA extracted from the brain stem and surrounding neural tissue clearly demonstrated that the immune responses after mRNA introduction were remarkably reduced by the use of polyplex nanomicelle compared with the administration of naked mRNA (Fig. 3). Indeed, naked mRNA induced significant immune responses, although it provided almost no

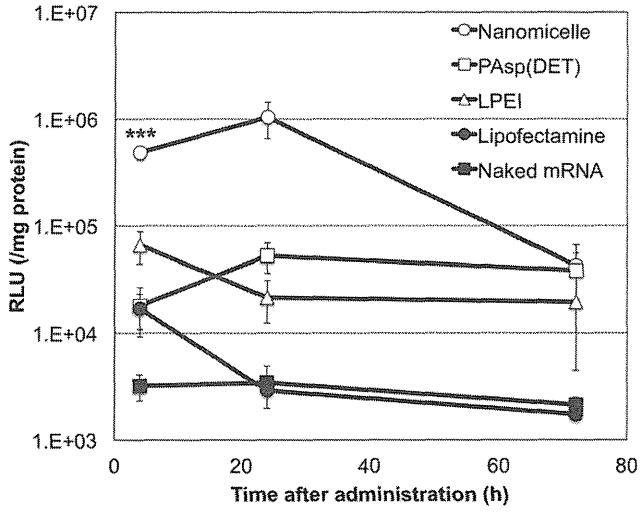

Figure 1. Time dependent profile of luciferase expression in CNS after mRNA administration. Ten μl of mRNA-containing carriers (2 μg mRNA) of polyplex nanomicelle composed of PEG–PAsp(DET) (open circle), polyplex formed with cationic polymer, PAsp(DET) (open square) and linear polyethyleneimine (LPEI) (open triangle), Lipofectamine 2000 (closed circle) and naked mRNA solution (closed square) were injected into the cisterna magna of mice. Luciferase expression was evaluated from the extracted brain and spinal tissues. The data are presented as the mean ± standard error of the mean (s.e.m.) (N≥5). Statistical significance was assessed by 2-tailed Student's t-test, ***, P<0.001 versus PAsp(DET), LPEI, Lipofectamine 2000 and naked mRNA groups. RLU, relative luminescence units.
doi:10.1371/journal.pone.0056220.g001

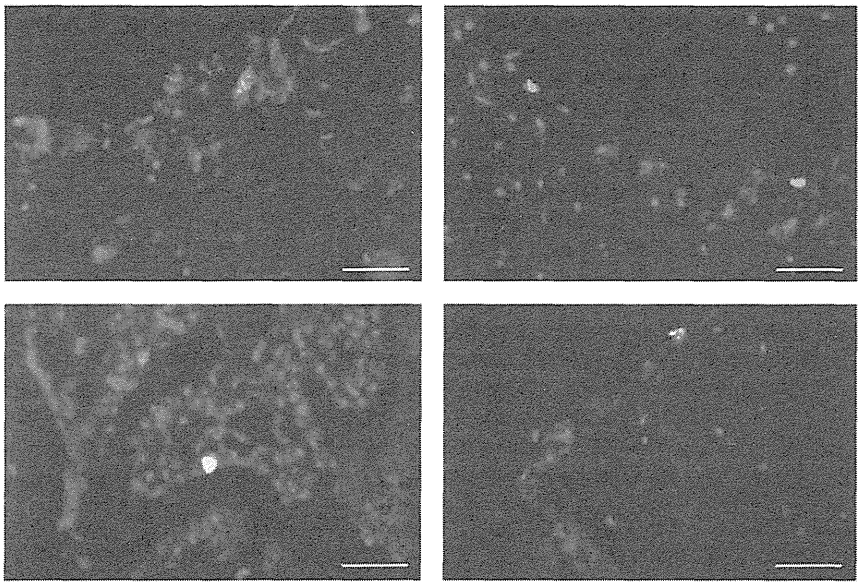

Figure 2. GFP expression in CNS after mRNA delivery using polyplex nanomicelle. Fluorescent microscopic images of brain tissue were taken 48 h after the administration of nanomicelle loading GFP-expressing mRNA. GFP was visualised by immunostaining using an anti-GFP monoclonal antibody (green). The cell nuclei were stained with Hoechst 33342 (blue). Scale bars: 20 μm.
doi:10.1371/journal.pone.0056220.g002

luciferase expression in CNS (Fig. 1). Note that cytokine production can properly be evaluated from the expression level of corresponding mRNAs by qPCR method according to the literature [35,36].

Comparison of modified and unmodified mRNA possessing identical sequences revealed that immune responses induced by naked unmodified mRNA were higher than those produced by modified mRNA (Fig. 3), confirming the ability of modification to reduce the immunogenicity of mRNA. However, the polyplex nanomicelle effectively suppressed immune responses even when using unmodified mRNA to the same extent as the modified mRNA.

For detailed evaluation of intracellular mechanisms, we focused on immune responses induced directly by recognition of mRNA by the innate immune systems. Exogenous mRNA is known to be recognised by TLRs, in particular, by TLR3, 7 and 8, that localize mainly on the membrane of the endosomes [37]. For this analysis, transformants of HEK293 cells that stably express a specific type of human TLR were used for *in vitro* mRNA transfection [23]. Since wild-type HEK293 cells have very low expression levels of endogenous TLRs, the transformants allowed us to analyse the specific recognition between exogenous mRNA and the specific type of TLR to induce the immune responses.

After transfection of mRNA (modified or unmodified) toward HEK293 transformant expressing human TLR7 (293-hTLR7), expression levels of inflammatory cytokine (IL-8) and type 1 interferon (IFN-β1) were measured 4 h after transfection. When using the nanomicelle, expression of IL-8 and IFN-β1 remained to the levels of nontransfected controls (Fig. 4). In contrast, after transfection of mRNA using Lipofectamine 2000 or as naked mRNA, significantly higher expression of IL-8 and IFN-β1 was induced in 293-hTLR7 cells. To confirm the specificity of mRNA recognition by TLR7, another type of transformant expressing human TLR9 (293-hTLR9), known to have specific affinity to double-stranded DNA (dsDNA) but not to mRNA [38], was used. For the 293-hTLR9 cells, almost no increase in expression of IL-8 and IFN-β1 was observed after transfection using naked mRNA as well as the nanomicelle (Fig. 4). In contrast, when using Lipofectamine 2000, IL-8 and IFN-β1 expression showed considerable upregulation compared with the controls, although the levels were remarkably lower than those in 293-hTLR7 cells. These tendencies were similarly observed for both modified and unmodified mRNA regardless of the transfection methods used.

To exclude the possibility that the differences in immune responses among the transfection methods were because of the differences in the amounts of cellular uptake of exogenous mRNA, we quantified the amounts by real-time quantitative PCR (RT-PCR) of total mRNA extracted from the transfected cells. Indeed, the amount of mRNA detected 4 h after transfection using the nanomicelle and Lipofectamine 2000 were approximately 1%–10% of the total dose of transfected mRNA, whereas the amount introduced by naked mRNA transfection was much lower by 4 digits (Fig. S3). Thus, these results strongly suggest that mRNA introduction in the form of naked mRNA as well as the introduction using Lipofectamine 2000 induced immune responses by recognition of mRNA by TLRs, where the degree of immune responses was a reflection of the amount of mRNA internalization into the cells. In contrast, the nanomicelle significantly reduced the mRNA-specific activation of TLR7 signalling even though the substantial amount of mRNA was internalised into the cells, indicating that the recognition of mRNA by TLR7 was effectively avoided by the use of nanomicelle.

Prolonged protein secretion into cerebrospinal fluid (CSF) was achieved by mRNA introduced by polyplex nanomicelle

Finally, we evaluated the properties of mRNA for prolonged protein secretion into CSF. mRNA expressing Gaussia luciferase (GLuc), a secreted type of luciferase, was incorporated in the polyplex nanomicelle and introduced into the subarachnoid space of rats by intrathecal injection. GLuc expression in the CSF was then measured [39]. For comparison, pDNA expressing GLuc was also examined after incorporation in the polyplex nanomicelle. In

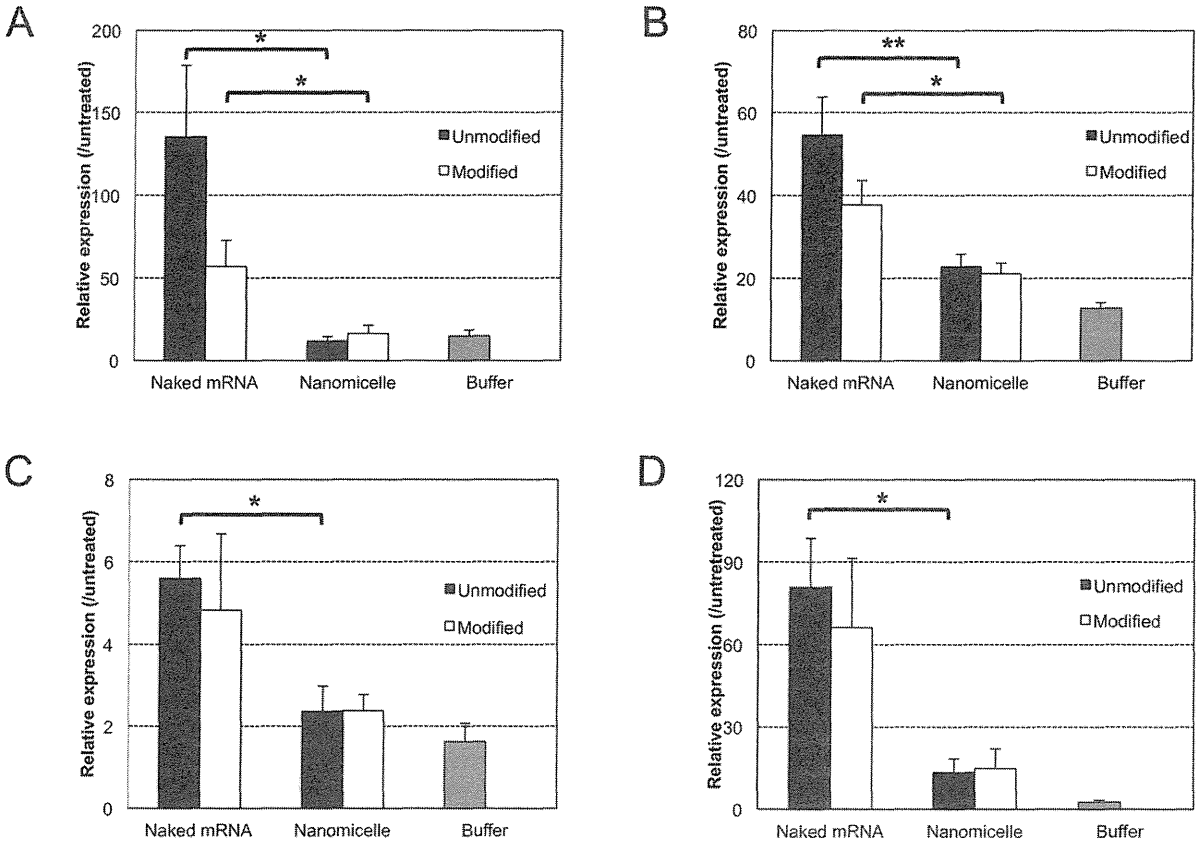

Figure 3. Evaluation of immune responses in CNS after mRNA delivery. mRNA (modified or unmodified) was administered into CNS either as a form of naked mRNA or using polyplex nanomicelle. Expression of proinflammatory cytokines of (a) interleukin (IL)-6, (b) tumour necrosis factor (TNF)-α, (c) interferon (IFN)-α4 and (d) IFN-β1 in the brain stem were measured using real-time quantitative PCR (RT-PCR) 4 h after administration. The data are presented as the mean ± standard errors of the mean (s.e.m.) (N≥4). Statistical significance was assessed by 2-tailed Student's t-test, *, $P<0.05$, **, $P<0.01$.
doi:10.1371/journal.pone.0056220.g003

addition, the proteinous form of GLuc was used after being collected from GLuc-expressing culture cells (Methods).

Time-dependent profiles of GLuc expression in CSF revealed that mRNA incorporated in the nanomicelle provided detectable expression in a sustained manner up to 120 h after introduction (Fig. 5). In contrast, after introduction of GLuc protein into the subarachnoid space, the protein rapidly decreased below detectable levels within 4 h after the introduction. pDNA showed prolonged GLuc expression for more than 120 h; however, mRNA showed 1-order higher GLuc expression 4 h after introduction.

Discussion

This study represents the advantages of the polyplex nanomicelle containing mRNA for providing therapeutic proteins and peptides to CNS by intrathecal injection. Various recombinant proteins are available and in use for clinical purposes; however, the functional duration of the proteins is very short because of their poor stability under physiological conditions, leading to inconsistent outcomes. Moreover, repeated protein administration is costly. Compared with *in vivo* protein delivery, mRNA is apparently advantageous for obtaining protein secretion in a sustained manner with much less frequent administration.

It is reasonable to claim that pDNA has an advantage over mRNA from the viewpoint of sustainable transgene expression because DNA is much more stable than mRNA under physiological conditions. However, pDNA introduction is destined to cause an inevitable risk of random integration into the genome because the risk cannot be decreased below the level of spontaneous genetic recombination. DNA introduction may be accepted only for cases such as fatal diseases in which the risk of random integration is compensated by the benefit of DNA introduction, leading to difficulty in clinical applications of DNA introduction or trials categorised as 'gene therapy'.

mRNA is a promising alternative to pDNA. As shown in Fig. 5, the very early onset of protein expression from mRNA provides a significant advantage over pDNA because mRNA does not need to be delivered into the nucleus. It is still challenging to obtain prolonged protein expression from mRNA to a comparable level as pDNA. Nevertheless, mRNA has simpler intracellular processes compared with pDNA. Thus, once the instability of mRNA can be sufficiently overcome by the polyplex nanomicelle, mRNA is likely to be advantageous to satisfy the various demands of therapeutic applications in a more flexible manner.

In this context, it is essential to regulate the immunogenicity of mRNA. The results of analysing immune responses both *in vivo* and *in vitro* (Fig. 3, 4) strongly suggested that the polyplex nanomicelle effectively suppressed the immune responses even when a considerable amount of mRNA was introduced into the cells. According to the results of naked mRNA, mRNA induced significant responses even with a very low amount of cellular uptake. The modification of mRNA could indeed reduce immune

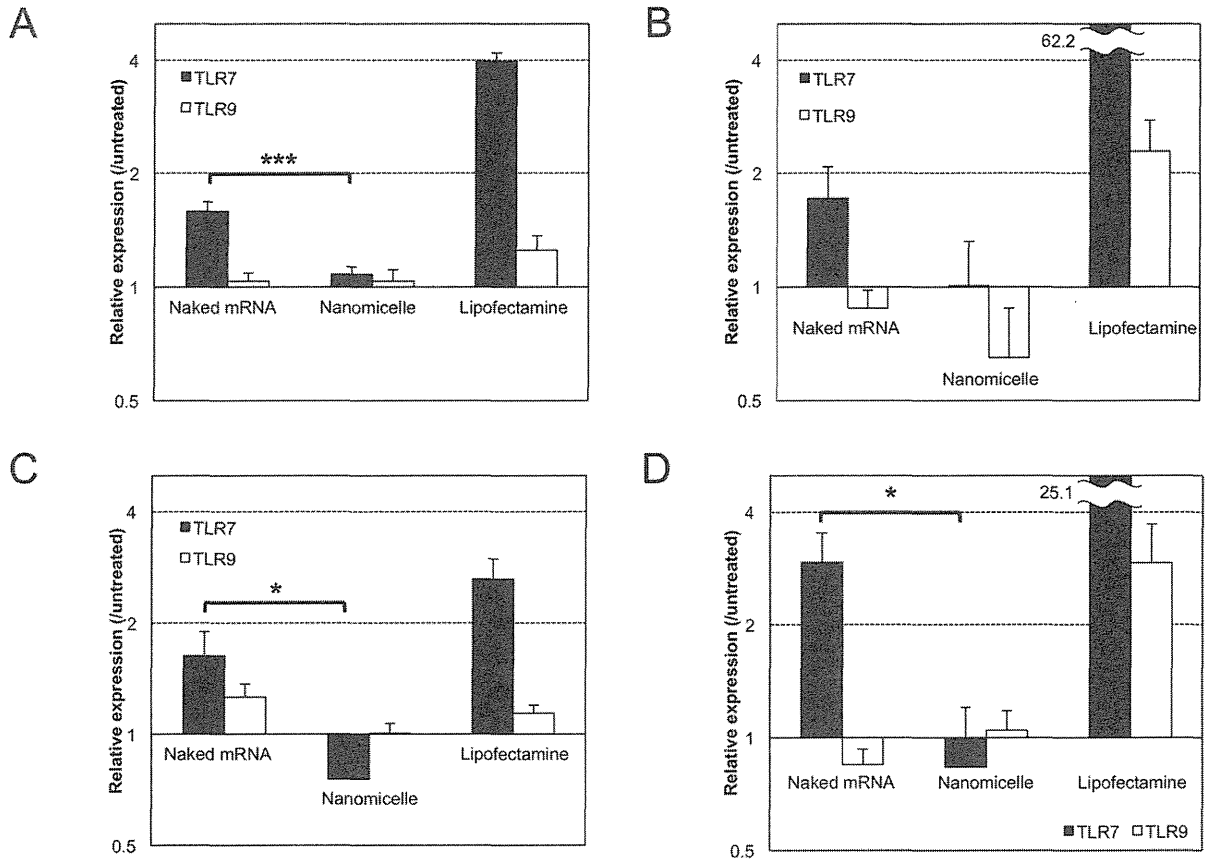

Figure 4. In vitro analysis of Toll-like receptor (TLR) signalling after mRNA introduction. To evaluate mRNA-mediated TLR signaling, HEK293 cells expressing TLR7 (grey bars) were used. HEK293 cells expressing TLR9 (white bars), which does not recognise mRNA, were also used as a negative control. Cells were treated with naked mRNA, polyplex nanomicelle or Lipofectamine 2000 using unmodified mRNA (a, b) or modified mRNA (c, d). Expression of interleukin (IL)-8 (a, c) and interferon (IFN)-β1 (b, d) was measured at transcriptional levels using real-time quantitative PCR (RT-PCR) 4 h after mRNA introduction. The data are presented as the mean ± standard error of the mean (s.e.m.) (N = 6). Statistical significance was assessed by 2-tailed Student's t-test, *, $P<0.05$, ***, $P<0.001$.
doi:10.1371/journal.pone.0056220.g004

responses; however it could not eliminate them completely. Eventually, the nanomicelle played an effective role in reducing immune responses even when unmodified mRNA was used. This result should be attributed to the stealth property of the nanomicelle of encapsulating mRNA shielded by the outer PEG layer [27]. Furthermore, the cationic polymer used in the polyplex nanomicelle PAsp(DET) has a strong capacity to promote the endosomal escape [32,40], thereby allowing the polyplex containing mRNA to smoothly travel through the endosomes without being recognised by TLRs.

Of noted, Lipofectamine 2000 induced strong immune responses after transfection toward 293-hTLR9 as well as 293-hTLR7 cells, although responses in the former were lower than those in the latter (Fig. 4). It is known that lipid-based reagents tend to destabilise the plasma membrane, facilitating the smooth internalisation of lipoplexes [41]. In addition, the facile disintegration of the lipoplexes to release the mRNA inside the cells contributed to efficient protein expression in *in vitro* settings [42]. However, these properties of lipoplexes may also increase the mRNA recognition by TLRs inside the cells. Furthermore, it is likely that not only specific mRNA recognition by TLR7 but a different factor that could affect TLR9, presumably the leakage of genomic DNA from other cells because of membrane destabilisation, were involved in immune responses observed after transfection using Lipofectamine 2000.

As demonstrated in this study, the polyplex nanomicelle successfully provided protein secretion into CSF continuously for up to 3 days after administration. To the best of our knowledge, this is the first report of prolonged protein expression in CNS for more than a few days by *in vivo* mRNA administration using a non-viral delivery system. The key feature responsible for these outcomes should be attributed to the almost complete suppression of mRNA immunogenicity, regardless of the modification of mRNA. The stable retention of mRNA inside the nanomicelle and smooth endosomal escape may contribute to reduce unfavorable recognition of mRNA by TLRs in the endosomes. In the future, the retention and release kinetics of mRNA inside the nanomicelle should be highly controlled by the sophisticated molecular design of the nanomicelle, as was the case in our previous efforts for the nanomicelle containing pDNA or short interfering RNA (siRNA) [40]. In this manner, we believe that even more prolonged expression from mRNA will be achieved using the polyplex nanomicelle system to fulfill the various needs of treatments and administration routes (systemic or local injection), opening the door to various new therapeutic strategies using mRNA.

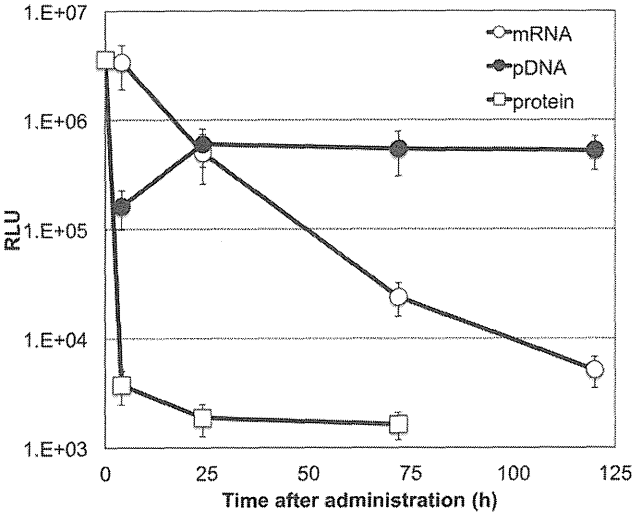

Figure 5. Comparison of mRNA, plasmid DNA (pDNA) and protein. mRNA or pDNA that expressed GLuc was incorporated in the polyplex nanomicelle and injected into the subarachnoid space of rats by intrathecal injection. The proteinous form of GLuc was also used for intrathecal injection. GLuc expression was evaluated from cerebrospinal fluid (CSF) collected at the indicated time points. The data are presented as the mean ± standard error of the mean (s.e.m.) (N = 4). RLU, relative luminescence units.
doi:10.1371/journal.pone.0056220.g005

Materials and Methods

Preparation of mRNA

For *in vitro* transcription (IVT) of luciferase, Gluc and GFP, the protein-expressing fragment of pGL4.13 (Promega, Madison, WI, USA), pCMV-Gluc control plasmid (New England BioLabs, Ipswich, MA, USA), and AcGFP vector (Clontech, Mountain View, CA, USA) respectively, were cloned into pSP73 vector (Promega) to give expression under a T7 promoter. pDNA was used as template for IVT after linearization by Nde I. IVT was performed using the mMESSAGE mMACHINE T7 Ultra Kit (Ambion, Invitrogen, Carlsbad, CA, USA), followed by polyadenylation using the poly(A) tail kit (Ambion). For mRNA modification, 5-methyl-CTP, pseudo-UTP and 2-thio-UTP (Tri-Link BioTechnologies, San Diego, CA, USA) were added to the reaction solution at compositions of 20%, 10% and 10% in total CTP or UTP, respectively, following the procedure reported previously [10]. Transcribed mRNA was purified with the RNeasy Mini Preparation Kit (Qiagen, Hilden, Germany). The mRNA concentration was determined spectroscopically at 260 nm.

Constructs for pDNA delivery

A protein-expressing fragment of pCMV-Gluc control plasmid were cloned into pCAG-GS (RIKEN, Tokyo, Japan) to provide expression under a CAG promoter/enhancer.

Preparation of polyplex nanomicelle and other carriers containing mRNA or pDNA

The PEG–PAsp(DET) block copolymer and PAsp(DET) homo polymer were synthesized as reported previously [30]. The PEG used in this study had a molecular weight (MW) of 12,000. By ^{1}H-NMR analyses, the polymerization degree of the PAsp(DET) portion was determined to be 57 for PEG–PAsp(DET) and 52 for PAsp(DET). Linear polyethyleneimine (LPEI) (ExGen 500 *in vivo*; MW = 22 kDa) was purchased from MBI Fermentas (Burlington, ON, Canada). For the preparation of the polyplex nanomicelle, PEG-PAsp(DET) polymer and nucleic acids (mRNA or DNA) was separately dissolved in 10 mM Hepes buffer. At this stage, the concentration of nucleic acid was set to 300 μg/ml, and that of PEG-PAsp(DET) was adjusted to obtain the ratio of amino groups in polymers to phosphate in mRNA or DNA (N/P ratio) to be 8. The solutions of PEG-PAsp(DET) polymer and nucleic acids were mixed by the volume ratio of 1:2, resulting in the polyplex nanomicelle solution containing 200 μg/ml of nucleic acids. PAsp(DET)-based mRNA carrier (N/P = 8) was prepared similarly as the polyplex nanomicelle. LPEI-based mRNA carrier was prepared following the manufacture's protocol at N/P ratio of 6. Lipofectamine 2000 (Invitrogen) and mRNA were mixed at the ratio indicated in the manufacturer's protocol. Final concentrations of nucleic acids (mRNA and pDNA) were adjusted to 200 μg/ml for all the samples.

Characterization of polyplex nanomicelle

The size and polydispersity index (PDI) of polyplex nanomicelle was measured by the dynamic light scattering measurement using Zetasizer Nanoseries (Malvern Instruments Ltd., UK) at a detection angle of 173° and a temperature of 25°C. After 3 times measurement of the sample, the data derived from the rate of decay in the photon correlation function were treated by a cumulant method, and the corresponding diameter of each sample was calculated according to the Stokes-Einstein equation. The nanomicelle was determined to have the size of 50.0 nm with a narrow distribution of polydispersity index = 0.19 (Fig. S1)

Preparation of Gluc protein solution

For the preparation of Gluc protein solution, *in vitro* transfection of GLuc-expressing pDNA was performed and the secreted GLuc protein was collected. HuH-7 cells were seeded at a density of 160,000 cells/well in 6-well culture plates. After 24 h of incubation in Dulbecco's Modified Eagle Medium (DMEM) (Sigma–Aldrich, St. Louis, MO, USA) containing 10% fetal bovine serum (FBS) (Life Technologies Japan Ltd., Tokyo, Japan) and 1% penicillin/streptomycin (Sigma–Aldrich), PAsp(DET)-based carriers loading pCAG-Gluc pDNA (N/P = 10) were added to each well (8 μg/well). After 24 h of transfection, the culture medium was replaced with phosphate-buffered saline (PBS), followed by incubation for 6 h. Following this, PBS containing GLuc protein was recovered and used as Gluc protein solution.

Intrathecal injection of carrier solution containing mRNA

BALB/c mice (female, 7 weeks old) and SD(IGS) rats (female, 8 weeks old) were purchased from Charles River Laboratories (Yokohama, Japan). Administration to neural tissues of mice was performed as described previously [43]. In brief, the mice were anaesthetized with 3% isoflurane (Abbott Japan Co., Ltd., Tokyo, Japan) and placed in a prone position with the neck bent forward. A 30-gauge needle was inserted into the cisterna magna from the space between occiput and C1, and 10 μl of solution containing 2 μg of mRNA was injected in 60 sec. For rats, meninges between occiput and C1 were exposed after anesthetizing by 3% isoflurane. A 30-gauge needle was inserted into the cisterna magna, and 50 μl of nanomicelle solution containing 10 μg of mRNA or pDNA, or Gluc protein solution was injected in 60 sec. CSF was collected from the cisterna magna in a similar manner by inserting a needle between occiput and C1. All animal protocols were conducted with the approval of the Animal Care and Use Committee, University of Tokyo, Japan.

Evaluation of luciferase expression in neural tissues

For evaluation of luciferase in the mice, the brain and spinal tissues were excised and thoroughly homogenized using a Multi-beads shocker (Yasui Kikai Corporation, Osaka, Japan). Luciferase expression was measured by the Luciferase assay system (Promega) using the Lumat LB9507 luminometer (Berthold, Bad Wildbad, Germany). The expression was represented after normalisation by total protein concentrations in the tissue lysates. For evaluation of GLuc (a secreted type of luciferase) in rats, CSF was collected, followed by measurement of expression using the Renilla Luciferase Assay system (Promega) and the Lumat LB9507 luminometer. Relative luminescence unit (RLU) value at 0 h of protein administration was plotted as 1/7 of RLU of the injected solution (50 μl) prepared from culture cells (described previously) because CSF volume of an adult rat is approximately 300 μl [44] and the solution was assumed to be diluted by 7 times. Indeed, it was confirmed that the CSF sample collected just after the administration of GLuc protein showed the expected RLU value of 1/7 of the injected solution (n = 1).

Immunohistological evaluation of neural tissue to analyse GFP expression

Brain tissues were harvested at 48 h after GFP-expressing mRNA administration, and 5-μm-thick frozen section were prepared by a method using an adhesive film [45]. GFP was immunostained with an anti-GFP monoclonal antibody (Invitrogen) at a dilution of 1:500 and an Alexa488-conjugated secondary antibody (Invitrogen, Carlsbad, CA, USA). After staining the nuclei with Hoechst 33342 (Dojindo, Kumamoto, Japan), the sections were observed with an Axiovert 200 fluorescence microscope (Carl Zeiss, Jena, Germany) using a 20× EC Plan Neofuar objective (Carl Zeiss).

Evaluation of immune responses in neural tissues

Total RNA was isolated from extracted neural tissues using the RNeasy Mini Preparation Kit. Gene expression of cytokines and interferons was analysed by RT-PCR using an ABI Prism 7500 Sequence Detector (Applied Biosystems, Foster City, CA, USA), and TaqMan Gene Expression Assays (Applied Biosystems, Mm00446190_m1 for interleukin (IL)-6, Mm00443258 for tumour necrosis factor (TNF)-α, Mm00439552_s1 for interferon (INF)-β1, Mm00833969_s1 for IFN-α4 and Mm00607939 for β-actin).

Analyses of exogenous mRNA recognition by TLRs in 293-hTLR7 and 293-hTLR9 cells

HEK293 cells stably transformed to express human TLR7 and TLR9 (InvivoGen, San Diego, CA, USA) were seeded at a density of 400,000 cells/well in 6-well culture plates and incubated in DMEM containing 10% FBS and 1% penicillin/streptomycin. After 24 h of incubation, the medium was replaced with serum free Opti-MEM medium (Invitrogen), and solution containing 8 μg of RNA encoding luciferase was added to each well. At 4 h after the addition of mRNA, total RNA was isolated from the cells using the RNeasy Mini Preparation Kit. Gene expression was analysed by RT-PCR using TaqMan Gene Expression Assays (Hs00174103_m1 for IL-8, Hs01077958_s1 for INF-β1 and 4310881E for β-actin). The cellular uptake of transfected mRNA was also quantified with RT-PCR by amplifying a 117-bp sequence in the luciferase gene using a forward primer, TGCAAAAGATCCTCAACGTG, and reverse primer, AATGG-GAAGTCACGAAGGTG.

Supporting Information

Figure S1 Size distribution of polyplex nanomicelle determined by dynamic light scattering (DLS).
(PDF)

Figure S2 Tissue distribution of luciferase expression after polyplex nanomicelle administration. Luciferase was extracted from the central nervous system (CNS) of mice at 4 h (closed bar) and 24 h (open bar) after the administration. The data are presented as the mean ± standard error of the mean (s.e.m.) (N = 6). RLU, relative luminescence units.
(PDF)

Figure S3 Cellular uptake of messenger RNA (mRNA) after *in vitro* delivery. HEK293 cells expressing Toll-like receptor (TLR) 7 were treated with naked mRNA, polyplex nanomicelle and Lipofectamine 2000-based carrier from unmodified mRNA. The amount of mRNA uptake was quantified at 4 h after the treatment using real-time quantitative PCR (RT-PCR). The data are presented as the mean ± standard error of the mean (s.e.m.) (N = 6).
(PDF)

Acknowledgments

We deeply appreciate Dr. Carsten Rudolph (Ludwig Maximilian's University Munich) for supplying technical information of mRNA modification. We also thank Ms. Tomoko Tamamoto, Yoko Hasegawa, Satomi Ogura, Asuka Miyoshi and Katsue Morii (The University of Tokyo) for technical assistance.

Author Contributions

Conceived and designed the experiments: SU KI KK. Performed the experiments: SU HU KH. Analyzed the data: SU KI. Contributed reagents/materials/analysis tools: TO TI SF KO. Wrote the paper: SU KI KK.

References

1. Callis J, Fromm M, Walbot V (1987) Expression of mRNA electroporated into plant and animal cells. Nucleic Acids Res 15: 5823–5831.
2. Malone RW, Felgner PL, Verma IM (1989) Cationic liposome-mediated RNA transfection. Proc Natl Acad Sci U S A 86: 6077–6081.
3. Tavernier G, Andries O, Demeester J, Sanders NN, De Smedt SC, et al. (2011) mRNA as gene therapeutic: how to control protein expression. J Control Release 150: 238–247.
4. Heil F, Hemmi H, Hochrein H, Ampenberger F, Kirschning C, et al. (2004) Species-specific recognition of single-stranded RNA via toll-like receptor 7 and 8. Science 303: 1526–1529.
5. Kariko K, Ni H, Capodici J, Lamphier M, Weissman D (2004) mRNA is an endogenous ligand for Toll-like receptor 3. J Biol Chem 279: 12542–12550.
6. Mitchell DA, Nair SK (2000) RNA-transfected dendritic cells in cancer immunotherapy. J Clin Invest 106: 1065–1069.
7. Van Tendeloo VF, Ponsaerts P, Berneman ZN (2007) mRNA-based gene transfer as a tool for gene and cell therapy. Curr Opin Mol Ther 9: 423–431.
8. Weide B, Carralot JP, Reese A, Scheel B, Eigentler TK, et al. (2008) Results of the first phase I/II clinical vaccination trial with direct injection of mRNA. J Immunother 31: 180–188.
9. Weide B, Pascolo S, Scheel B, Derhovanessian E, Pflugfelder A, et al. (2009) Direct injection of protamine-protected mRNA: results of a phase 1/2 vaccination trial in metastatic melanoma patients. J Immunother 32: 498–507.
10. Kormann MS, Hasenpusch G, Aneja MK, Nica G, Flemmer AW, et al. (2011) Expression of therapeutic proteins after delivery of chemically modified mRNA in mice. Nat Biotechnol 29: 154–157.
11. Kariko K, Muramatsu H, Keller JM, Weissman D (2012) Increased Erythropoiesis in Mice Injected With Submicrogram Quantities of Pseudouridine-containing mRNA Encoding Erythropoietin. Mol Ther 20: 948–953.

12. Brennan CM, Steitz JA (2001) HuR and mRNA stability. Cell Mol Life Sci 58: 266–277.
13. Rejman J, Tavernier G, Bavarsad N, Demeester J, De Smedt SC (2010) mRNA transfection of cervical carcinoma and mesenchymal stem cells mediated by cationic carriers. J Control Release 147: 385–391.
14. Plews JR, Li J, Jones M, Moore HD, Mason C, et al. (2010) Activation of pluripotency genes in human fibroblast cells by a novel mRNA based approach. PLoS One 5: e14397.
15. Warren L, Manos PD, Ahfeldt T, Loh YH, Li H, et al. (2010) Highly efficient reprogramming to pluripotency and directed differentiation of human cells with synthetic modified mRNA. Cell Stem Cell 7: 618–630.
16. Tavernier G, Wolfrum K, Demeester J, De Smedt SC, Adjaye J, et al. (2011) Activation of pluripotency-associated genes in mouse embryonic fibroblasts by non-viral transfection with in vitro-derived mRNAs encoding Oct4, Sox2, Klf4 and cMyc. Biomaterials.
17. Wolff JA, Malone RW, Williams P, Chong W, Acsadi G, et al. (1990) Direct gene transfer into mouse muscle in vivo. Science 247: 1465–1468.
18. Probst J, Weide B, Scheel B, Pichler BJ, Hoerr I, et al. (2007) Spontaneous cellular uptake of exogenous messenger RNA in vivo is nucleic acid-specific, saturable and ion dependent. Gene Ther 14: 1175–1180.
19. Qju P, Ziegelhoffer P, Sun J, Yang NS (1996) Gene gun delivery of mRNA in situ results in efficient transgene expression and genetic immunization. Gene Ther 3: 262–268.
20. Scheel B, Teufel R, Probst J, Carralot JP, Geginat J, et al. (2005) Toll-like receptor-dependent activation of several human blood cell types by protamine-condensed mRNA. Eur J Immunol 35: 1557–1566.
21. Zou S, Scarfo K, Nantz MH, Hecker JG (2010) Lipid-mediated delivery of RNA is more efficient than delivery of DNA in non-dividing cells. Int J Pharm 389: 232–243.
22. Su X, Fricke J, Kavanagh DG, Irvine DJ (2011) In Vitro and in Vivo mRNA Delivery Using Lipid-Enveloped pH-Responsive Polymer Nanoparticles. Mol Pharm 8: 774–787.
23. Kariko K, Buckstein M, Ni H, Weissman D (2005) Suppression of RNA recognition by Toll-like receptors: the impact of nucleoside modification and the evolutionary origin of RNA. Immunity 23: 165–175.
24. Anderson BR, Muramatsu H, Nallagatla SR, Bevilacqua PC, Sansing LH, et al. (2010) Incorporation of pseudouridine into mRNA enhances translation by diminishing PKR activation. Nucleic Acids Res 38: 5884–5892.
25. Kariko K, Muramatsu H, Welsh FA, Ludwig J, Kato H, et al. (2008) Incorporation of pseudouridine into mRNA yields superior nonimmunogenic vector with increased translational capacity and biological stability. Mol Ther 16: 1833–1840.
26. Charette M, Gray MW (2000) Pseudouridine in RNA: what, where, how, and why. IUBMB Life 49: 341–351.
27. Itaka K, Kataoka K (2009) Recent development of nonviral gene delivery systems with virus-like structures and mechanisms. Eur J Pharm Biopharm 71: 475–483.
28. Abbott NJ (2004) Evidence for bulk flow of brain interstitial fluid: significance for physiology and pathology. Neurochem Int 45: 545–552.
29. Kataoka K, Harada A, Nagasaki Y (2001) Block copolymer micelles for drug delivery: design, characterization and biological significance. Adv Drug Deliv Rev 47: 113–131.
30. Kanayama N, Fukushima S, Nishiyama N, Itaka K, Jang WD, et al. (2006) A PEG-based biocompatible block catiomer with high buffering capacity for the construction of polyplex micelles showing efficient gene transfer toward primary cells. ChemMedChem 1: 439–444.
31. Itaka K, Kataoka K (2011) Progress and prospects of polyplex nanomicelles for plasmid DNA delivery. Curr Gene Ther 11: 457–465.
32. Miyata K, Oba M, Nakanishi M, Fukushima S, Yamasaki Y, et al. (2008) Polyplexes from poly(aspartamide) bearing 1,2-diaminoethane side chains induce pH-selective, endosomal membrane destabilization with amplified transfection and negligible cytotoxicity. J Am Chem Soc 130: 16287–16294.
33. Masago K, Itaka K, Nishiyama N, Chung UI, Kataoka K (2007) Gene delivery with biocompatible cationic polymer: pharmacogenomic analysis on cell bioactivity. Biomaterials 28: 5169–5175.
34. Itaka K, Ishii T, Hasegawa Y, Kataoka K (2010) Biodegradable polyamino acid-based polycations as safe and effective gene carrier minimizing cumulative toxicity. Biomaterials 31: 3707–3714.
35. Giulietti A, Overbergh L, Valckx D, Decallonne B, Bouillon R, et al. (2001) An overview of real-time quantitative PCR: applications to quantify cytokine gene expression. Methods 25: 386–401.
36. Listvanova S, Temmerman S, Stordeur P, Verscheure V, Place S, et al. (2003) Optimal kinetics for quantification of antigen-induced cytokines in human peripheral blood mononuclear cells by real-time PCR and by ELISA. J Immunol Methods 281: 27–35.
37. Krieg AM, Vollmer J (2007) Toll-like receptors 7, 8, and 9: linking innate immunity to autoimmunity. Immunol Rev 220: 251–269.
38. Akira S, Takeda K, Kaisho T (2001) Toll-like receptors: critical proteins linking innate and acquired immunity. Nat Immunol 2: 675–680.
39. Tannous BA (2009) Gaussia luciferase reporter assay for monitoring biological processes in culture and in vivo. Nat Protoc 4: 582–591.
40. Miyata K, Nishiyama N, Kataoka K (2012) Rational design of smart supramolecular assemblies for gene delivery: chemical challenges in the creation of artificial viruses. Chem Soc Rev 41: 2562–2574.
41. Lv H, Zhang S, Wang B, Cui S, Yan J (2006) Toxicity of cationic lipids and cationic polymers in gene delivery. J Control Release 114: 100–109.
42. Bettinger T, Carlisle RC, Read ML, Ogris M, Seymour LW (2001) Peptide-mediated RNA delivery: a novel approach for enhanced transfection of primary and post-mitotic cells. Nucleic Acids Res 29: 3882–3891.
43. Reijneveld JC, Taphoorn MJ, Voest EE (1999) A simple mouse model for leptomeningeal metastases and repeated intrathecal therapy. J Neurooncol 42: 137–142.
44. Veening JG, Barendregt HP (2010) The regulation of brain states by neuroactive substances distributed via the cerebrospinal fluid; a review. Cerebrospinal Fluid Res 7: 1.
45. Kawamoto T (2003) Use of a new adhesive film for the preparation of multi-purpose fresh-frozen sections from hard tissues, whole-animals, insects and plants. Arch Histol Cytol 66: 123–143.

frontiers in ONCOLOGY

REVIEW ARTICLE
published: 31 January 2013
doi: 10.3389/fonc.2013.00008

Response to DNA damage: why do we need to focus on protein phosphatases?

Midori Shimada* and Makoto Nakanishi*

Department of Cell Biology, Graduate School of Medical Sciences, Nagoya City University, Nagoya, Japan

Edited by:
Mira Jung, Georgetown University, USA

Reviewed by:
Fatih Uckun, University of Southern California, USA
Zhenkun Lou, Mayo Clinic, USA

****Correspondence:***
Midori Shimada and Makoto Nakanishi, Department of Cell Biology, Graduate School of Medical Sciences, Nagoya City University, 1-Kawasumi, Mizuho-cho, Mizuho-ku, Nagoya 467-8601, Japan.
e-mail: midorism@med.nagoya-cu.ac.jp; mkt-naka@med.nagoya-cu.ac.jp

Eukaryotic cells are continuously threatened by unavoidable errors during normal DNA replication or various sources of genotoxic stresses that cause DNA damage or stalled replication. To maintain genomic integrity, cells have developed a coordinated signaling network, known as the DNA damage response (DDR). Following DNA damage, sensor molecules detect the presence of DNA damage and transmit signals to downstream transducer molecules. This in turn conveys the signals to numerous effectors, which initiate a large number of specific biological responses, including transient cell cycle arrest mediated by checkpoints, DNA repair, and apoptosis. It is recently becoming clear that dephosphorylation events are involved in keeping DDR factors inactive during normal cell growth. Moreover, dephosphorylation is required to shut off checkpoint arrest following DNA damage and has been implicated in the activation of the DDR. Spatial and temporal regulation of phosphorylation events is essential for the DDR, and fine-tuning of phosphorylation is partly mediated by protein phosphatases. While the role of kinases in the DDR has been well documented, the complex roles of protein dephosphorylation have only recently begun to be investigated. Therefore, it is important to focus on the role of phosphatases and to determine how their activity is regulated upon DNA damage. In this work, we summarize current knowledge on the involvement of serine/threonine phosphatases, especially the protein phosphatase 1, protein phosphatase 2A, and protein phosphatase Mg^{2+}/Mn^{2+}-dependent families, in the DDR.

Keywords: DNA damage response, phosphorylation, protein phosphatase, DNA repair, chromatin

INTRODUCTION

The DNA damage response (DDR) signaling network mediates a wide variety of cellular events, including DNA repair, cell cycle arrest, apoptosis, and premature senescence, to maintain genomic integrity. Loss of checkpoint function results in chromosomal instability and aneuploidy, which promote tumorigenesis, suggesting that proper checkpoint signaling is essential for preventing cancer. From recent studies, it has become clear that protein phosphorylation plays a major role in the regulation of diverse DDR pathways. The initiation of some DDR processes is mainly mediated by protein kinases in the phosphoinositide 3-kinase (PI3-K)-related kinase family, as well as ataxia-telangiectasia mutated (ATM), ATM and Rad3-related (ATR), and DNA-dependent protein kinase (DNA-PK). These kinases orchestrate the cellular responses to DNA damage and activate the multiple cascades involved in the DDR through phosphorylation of a variety of substrates (Shiloh, 2003). Effector kinases, Chk1 and Chk2, are activated mainly by ATR and ATM, respectively, and transmit signals to a variety of downstream factors, such as p53, pRB, and Cdc25, ultimately leading to inactivation of cyclin-dependent kinases (Cdks) and inhibiting cell-cycle progression. Thus, studies have demonstrated that protein phosphorylation, mainly at serine (S)/threonine (T) residues, is essential for the DDR and regulates enzymatic activity, localization, protein–protein interactions, and stabilization. Given the fact that ATM and ATR are known to have hundreds of substrates, a large number of phosphorylation events are regulated and have roles in the DDR, although the biological significance of many of these phosphorylation events is largely unknown. Indeed, the catalytic subunits of protein phosphatases and their regulators are also targets of ATM and ATR, suggesting that the activity of protein phosphatases is regulated by phosphorylation during the DDR.

Recent large proteomic analyses have revealed that most phosphorylation events are tightly regulated both spatially and temporally, suggesting that a comprehensive analysis of the timing and location of phosphorylation events, rather than analysis of phosphorylation levels in whole cells, is essential to understand the DDR. In recent years, it has become increasingly clear that phosphatases, particularly S/T phosphatases, regulate the DDR not only by counteracting the function of kinases, but also by initiation of specific steps during the DDR. Given that fine-tuning of phosphorylation events is partly mediated by phosphatases, studies should focus on the involvement of protein phosphatases in the DDR and how their activity is regulated *in vivo*. In addition to phosphorylation, different types of post-translational modifications also have important roles in the DDR. Thus, it will be important to investigate the correlation between phosphorylation/dephosphorylation and other types of modifications. In this study, we summarize recent reports that have revealed new functions of S/T phosphatases in the DDR.

INTRODUCTION TO THE DDR

Upon formation of DNA double-strand breaks (DSBs), ATM is autophosphorylated at S1981 and then dissociates from an inactive homodimer into active monomers (Bakkenist and Kastan, 2003). It has been reported that phosphorylation of ATM on S367, S1893, and S1981 is required for ATM activation in human cells (Bakkenist and Kastan, 2003; Kozlov et al., 2006). Contrary to these findings, corresponding phosphorylation of these sites are dispensable for murine ATM activation (Pellegrini et al., 2006; Daniel et al., 2008). Instead of ATM activation, S1981 phosphorylation is required for ATM retention at sites of DSBs through interaction with mediator of DNA damage checkpoint 1 (MDC1; So et al., 2009). ATM is recruited to DSBs and activated by the MRN complex (Mre11, Rad50, and NBS1) through the association with NBS1 (Uziel et al., 2003; Falck et al., 2005; Lee and Paull, 2005). In response to DSBs, ATM phosphorylates histone H2AX at S139 (termed γ-H2AX), which extends up to megabases away from break sites that are readily visible as foci by immunofluorescence microscopy (Burma et al., 2001; Ward and Chen, 2001; Shroff et al., 2004; Stiff et al., 2004). These γ-H2AX foci are colocalized with many proteins involved in the DDR, such as MDC1, 53BP1, BRCA1, and the MRN complex (Paull et al., 2000). Indeed, γ-H2AX is required for the recruitment and maintenance of these factors at damaged sites in order to transmit signals to downstream factors.

Following single-stranded DNA (ssDNA) damage, replication defects, or during the process of DSBs, ATR, which forms a complex with ATRIP, is recruited to the region of replication protein A (RPA)-coated ssDNA (Zou and Elledge, 2003). Rad17, associated with small subunits of replication factor C (RFC), recognizes the junctions between ssDNA and dsDNA and facilitates the loading of the Rad9-Rad1-Hus1 (9-1-1 complex) sliding clamp onto the DNA (Kondo et al., 2001; Melo et al., 2001; Zou and Elledge, 2003). In concert with ATR/ATRIP and RPA, the 9-1-1 complex appears to act as a sensor of DNA damage and interacts with TopBP1, thereby loading it onto sites of DNA damage. Rad17 interacts with Claspin to promote the phosphorylation of Chk1 (Roos-Mattjus et al., 2002; Bermudez et al., 2003; Wang et al., 2006). All of these proteins, i.e., ATRIP, RPA, RAD17, the 9-1-1 complex, and TopBP1, are phosphorylated by ATR during checkpoint activation. Through an interaction with TopBP1, ATR becomes fully active, thereby inducing subsequent responses (Delacroix et al., 2007; Lee et al., 2007a).

ATR and ATM phosphorylate and activate the effector kinases Chk1 and Chk2, respectively. Chk1 is composed of N-terminal catalytic domain and a regulatory C-terminus, which negatively regulates Chk1 kinase activity. Several reports have identified the functional roles of Chk1 phosphorylation *in vivo*. In response to cellular stresses, Chk1 phosphorylation occurs primarily on 2 residues, S317 and S345 (Liu et al., 2000; Zhao and Piwnica-Worms, 2001). Phosphorylated Chk1 is released from chromatin and accumulates in the cytoplasm to prevent activation of Cdk1 and entry into mitosis (Kramer et al., 2004). Phosphorylation of the C-terminal residues (mainly S317 and S345) block intramolecular interactions, reversing this autoinhibition mechanism (Katsuragi and Sagata, 2004). Regardless of this negative regulatory mechanism, Chk1 has basal activity in its unmodified form, and this activity is sufficient to phosphorylate several substrates, including histone H3 at T11 and Aurora B (Falck et al., 2005; Shimada et al., 2008). Thus, phosphorylation of S317 and S345 induces conformational changes that permit full activation and spatiotemporal regulation of Chk1 (Katsuragi and Sagata, 2004; Ng et al., 2004; Clarke and Clarke, 2005; Smits et al., 2006; Loffler et al., 2007; Niida et al., 2007). Upon DSBs, Chk2 is phosphorylated at T68 by ATM, which triggers Chk2 dimerization and activation by autophosphorylation of residues T383 and T387 in the T-loop (Ahn et al., 2000; Melchionna et al., 2000; Xu et al., 2002). Given that chromatin-bound Chk2 is dissociated from chromatin in response to ionizing radiation (IR), this notion also suggests that Chk2, when localized other than undamaged sites, may allow further activation of downstream effectors (Li and Stern, 2005). Although biochemical analyses revealed that Chk2 can phosphorylate Cdc25A, Cdc25C, BRCA1, and p53, examination of Chk2-deficient mice and cells showed that Chk2 functions mainly in p53-dependent apoptosis (Jack et al., 2002). It is noteworthy that Chk2 and Chk1 have partially redundant roles and share multiple substrates (Bartek and Lukas, 2003; Uziel et al., 2003; Lee and Paull, 2005). However, despite their overlapping roles in checkpoint signaling, the biological requirements for Chk1 and Chk2 function are strikingly different (Bartek and Lukas, 2003). In any case, these checkpoint kinases phosphorylate effector molecules, such as p53 and Cdc25 proteins, to induce cell cycle arrest (Sanchez et al., 1997; Hirao et al., 2000; Shieh et al., 2000; Falck et al., 2001).

DNA-dependent protein kinase plays a critical role in DNA damage repair, especially in non-homologous end-joining (NHEJ) repair of DSBs. DNA-PK is composed of three factors, a catalytic subunit (DNA-PKcs), Ku70, and Ku80, the latter two of which form a Ku heterodimer, and is essential for NHEJ to repair DNA DSBs. The Ku70/Ku80 heterodimer first binds to each broken DNA strand, after which DNA-PKcs is recruited to the DNA ends through interaction with the Ku heterodimer (Gottlieb and Jackson, 1993), promoting DNA repair. Importantly, DNA-PKcs is autophosphorylated at multiple sites and the regions of 2023–2056 and 2609–2647 are identified as major autophosphorylation clusters (Ding et al., 2003; Block et al., 2004; Chen et al., 2005; Cui et al., 2005). Among them, S2056 and T2609 are phosphorylated following IR and extensively studied. Such autophosphorylation of DNA-PKcs is important for end processing, disassembly, and inactivation (Merkle et al., 2002). Functional analysis using hypo- or hyperphosphorylated mutations of DNA-PKcs suggest that timely phosphorylation and dephosphorylation are essential for its function (Chan et al., 2002).

DYNAMIC CHANGES IN PROTEIN PHOSPHORYLATION FOLLOWING DNA DAMAGE

Protein phosphorylation is one of the most common post-translational modifications and is known to control many cellular processes. The phosphorylation state of a protein represents a balance between the activity of protein kinases and protein phosphatases. It has been reported that one-third of cellular proteins are phosphorylated, and more than 98% of protein phosphorylation

occurs on S and T residues (Olsen et al., 2006). Recently, several large-scale proteomic studies have revealed that ATM and ATR phosphorylate hundreds of proteins, which are involved in proliferation, cell structure, transcription, metabolic signaling, and RNA splicing (Matsuoka et al., 2007; Smolka et al., 2007; Stokes et al., 2007; Virshup and Shenolikar, 2009). Thus, ATM and ATR coordinate a much wider variety of cellular activities than initially expected. Protein phosphatase catalytic subunits and a number of their regulators were identified by these screens, suggesting that they play a role in the DDR downstream of ATM/ATR, although the functional meaning of these phosphorylation events has not been investigated. Large phosphoproteomic analyses performed in later studies reported dynamic and temporal aspects of phosphorylation and dephosphorylation following DSBs (Bennetzen et al., 2010; Bensimon et al., 2010). Bennetzen et al. (2010) classified the temporal profiles of nearly 600 regulated phosphorylation sites on 209 proteins and revealed that sites phosphorylated shortly after DSBs are enriched in SQ motifs, which are targets of ATM/ATR/DNA-PK, and in novel SXXQ motifs. Importantly, they identified a considerable number of sites that are dephosphorylated immediately after DNA damage. Bensimon et al. (2010) also performed quantitative phosphoproteomics and showed that 40% of DSB-induced phosphorylation events are ATM-independent. In addition, among ATM-dependent phosphorylation events, 75% are not located in SQ/TQ motifs, indicating the involvement of additional kinases activated by ATM. Similar to the results described by Bennetzen et al. (2010), Bensimon et al. (2010) found that more than 300 sites are dephosphorylated following DSBs among approximately 750 regulated phosphorylation sites on nearly 400 proteins; however, the functions of most of these dephosphorylation events have not yet been identified. Protein phosphatases contribute to shutting off DSB-induced phosphorylation during the late DDR; thus, these proteomic analyses suggested an additional function of phosphatases, which play a primary role in initiating some DDR processes.

PROTEIN PHOSPHATASES

The mammalian genome encodes nearly 500 protein kinases, 400 of which are S/T kinases. In contrast, the number of protein phosphatase catalytic subunits (e.g., catalytic subunit of PP1 is referred as PP1C) has been estimated to be 147, of which only about 40 are S/T phosphatases (Moorhead et al., 2007). The fact that so few S/T phosphatases counteract hundreds of distinct S/T kinases can be explained by the ability of phosphatases to form distinct components *in vivo*. Based on sequence, structure, and biological properties, S/T phosphatases can be classified into Mg^{2+}/Mn^{2+}-dependent phosphatases (PPMs) and the more diverse phosphoprotein phosphatases (PPPs). Among the PPP family, PP1 and PP2A are the most abundant isoforms, and their substrates have been relatively well characterized. PP1 and PP2A catalytic subunits interact with a vast number of regulators that target them to specific locations, mediate substrate specificity, and fine-tune phosphatase activity. In fact, mammalian cells contain more than 600 distinct PP1 complexes and approximately 70 PP2A holoenzymes (Ding et al., 2003).

PP1

PP1 catalyzes the majority of protein dephosphorylation events that regulate diverse cellular processes, such as neuronal signaling, muscle contraction, glycogen synthesis, and cell proliferation. Mammals have three PP1 catalytic genes, PP1α, -γ, and -δ, which encode very closely related proteins showing more than 85% similarity, with minor differences primarily at their NH_2 and COOH termini (Cohen, 2002). PP1γ has 2 isoforms, γ1 and γ2, generated by differential splicing of PP1γ. PP1 isoforms are expressed in all tissues and are widely distributed, except for PP1γ2, which is found only in the testes (Shima et al., 1993). PP1 isoforms show distinct subcellular localization, suggesting distinct roles and substrates for these enzymes (Andreassen et al., 1998). However, only a few reports have demonstrated specific differences for PP1 isoforms, since they do not show strict substrate specificities *in vitro* and have overlapping functions in most cases. Specificity is provided to PP1C through association with a large number of regulatory subunits that target catalytic subunits to specific subcellular localization, modulate their activity, and determine substrate specificity. Importantly many proteins involved in the DDR, including BRCA1, pRB, 53BP1, and Cdc25, harbor a PP1c-binding motif, RVxF (Ding et al., 2003; Kuntziger et al., 2011), and are targets of PP1.

The activity of PP1 is regulated by regulatory subunits such as protein phosphatase 1 nuclear targeting subunit (PNUTS), nuclear inhibitor of protein phosphatase 1 (NIPP1), inhibitor 2 (I2), and recruits PP1 onto mitotic chromatin at anaphase (RepoMan). Most forms of regulation are also achieved through the regulatory subunits; however, phosphorylation of PP1 by Cdk is also important for its activity. Nuclear PP1 shows higher activity in G_0/G_1 and G_2/M, and this change can be explained by Cdk-dependent phosphorylation of PP1 in its C-terminus. Cdk phosphorylates PP1α on T320, reducing its activity (Dohadwala et al., 1994; Berndt et al., 1997; Kwon et al., 1997). The equivalent T residue is conserved in all three PP1 isoforms (T316 in PP1β and T311 in PP1γ), and indeed, PP1γ is also inactivated by Cdk-dependent T311 phosphorylation (Shimada et al., 2010). Mice with depleted PP1γ are viable, but males show defective spermiogenesis and are infertile (Varmuza et al., 1999). These findings suggest that PP1α and/or -β could compensate for the depletion of PP1γ in development, but not in the specific function of spermiogenesis.

THE PP2A FAMILY

PP2 is further divided into three groups on the basis of metal-dependence: metal-independent PP2A, PP4, PP5, and PP6; Ca^{2+}-dependent PP2B and PP7; and Mg^{2+}/Mn^{2+}-dependent PP2C. Among the metal-independent group members, PP4 and PP6 share high homology with PP2A and are referred as PP2A-like phosphatases. Recent reports revealed that PP2A-like phosphatases have overlapping substrates and roles in the DDR.

PP2A

PP2A often functions as a heterotrimer, comprising three subunits designated A, B, and C. The core enzyme consists of the catalytic C subunit, scaffold A subunit, and variable regulatory B subunit. The regulatory B subunit defines the substrate specificity of the

PP2A holoenzyme and comprises four families: PR55/B (B55), PR61/ B′ (B56), PR72/B″, and striatins/SG2NA/B‴. Each one of these families contains various isoforms, which, when combined with the isoforms of both A and C subunits, produce a variety of PP2A holoenzymes that perform distinct functions. Depletion or inhibition of PP2A activity in *Xenopus* egg extracts inhibits the initiation of DNA replication by preventing binding of the initiation factor Cdc45 onto prereplication complexes (Lin et al., 1998; Chou et al., 2002). Additionally, recent studies have uncovered important roles for PP2A in the DDR. For example, PP2A is essential for the activation of ATM, ATR, Chk1, Chk2, and p53 and mediates G_2/M checkpoint control through regulation of the phosphorylation states of these proteins, although phosphorylation of Chk2 at T68, ATR at S428, and Chk1 at S317 is observed even in irradiated cells lacking PP2A activity (Yan et al., 2010).

PP4

PP4 is structurally and functionally related to PP2A and shares 65% amino acid identity with PP2A. PP4c associates with the regulatory subunits PP4R1, PP4R2, PP4R3α, PP4R3β, and PP4R4 (Cohen et al., 2005; Chen et al., 2008). Recent reports have demonstrated that PP4 possesses various cellular functions, including roles in nucleation, growth, and stabilization of microtubules at centrosomes/spindle bodies during cell division (Brewis et al., 1993; Helps et al., 1998; Hastie et al., 2000; Sumiyoshi et al., 2002). PP4 is localized predominantly to the nucleus, but some PP4 is present in cytoplasm and in mitotic centrosomes. Importantly, depletion of PP4 leads to embryonic lethality in mice, and PP4 deficiency in thymocytes results in decreased proliferation, indicating the essential role of PP4 in development and cell growth (Shui et al., 2007). Thanks to the functional analysis of newly identified PP4 substrates, our understanding of the role of PP4 in the DDR has also grown. Indeed, PP4 is involved in recovery from the G2/M checkpoint arrest after IR and required for cell survival in the presence of DNA replication inhibitors (Chowdhury et al., 2008; Nakada et al., 2008).

PP5

Unlike other related phosphatases, PP5 contains tetratricopeptide repeat (TPR) domains at the N-terminus. A catalytic domain and an auto-inhibitory domain are located at the C-terminus (Chinkers, 2001). Moreover, unlike other related phosphatases, whose substrate specificity is mediated by regulatory subunits, PP5 is regulated by protein–protein interactions through the TPR motif. Thus far, PP5 has been reported to interact with several proteins involved in the regulation of steroid signaling (Chen et al., 1996; Silverstein et al., 1997), cell cycle progression (Ollendorff and Donoghue, 1997; Zuo et al., 1998), and apoptosis (Morita et al., 2001) via the TPR domain. In addition, PP5 has been reported to be less abundant than other phosphatases, and has been shown to have low basal activity (Chinkers, 2001). PP5 knockout mice are viable, and the replication checkpoint is intact; however, the G_2/M checkpoint is impaired in PP5-knockout mouse embryonic fibroblasts (MEFs), indicating the essential function of PP5 in the DDR as general regulator of ATM, ATR, DNA-PK, or their substrates, as discussed below (Yong et al., 2007).

PP6

PP6 forms stable heterotrimers, comprising the PP6 catalytic subunit (PP6c), one of the three regulatory subunits (PP6R1, PP6R2, or PP6R3), and one of the three ankyrin repeat-containing subunits (ARS-A, ARS-B, or ARS-C; Stefansson and Brautigan, 2006; Stefansson et al., 2008). Functional analysis of PP6 showed that PP6 regulates G_1 to S progression through controlling cyclin D1 protein expression (Stefansson and Brautigan, 2007) and mitotic spindle formation through inhibition of an essential mitotic kinase, Aurora A (Zeng et al., 2010). Knockdown of either PP6R1 or PP6c impairs DNA-PK activation, DSB repair, and IR sensitivity, indicating that PP6 has critical roles in the DDR (Mi et al., 2009b; Douglas et al., 2010; Zhong et al., 2011).

PP2C

Wip1/PPM1D

PP2C belongs to the Mn^{2+}/Mg^{2+}-dependent PPM family. Unlike the PPP family, PP2C phosphatases are insensitive to inhibition by okadaic acid (OA) or microcystin and do not have regulatory subunits, but instead contain specific regulatory and targeting domains. Among the PP2C phosphatases, wild-type p53-inducible phosphatase 1 (Wip1), also termed PPM1D, which was originally identified in a screen for p53 target genes (Fiscella et al., 1997), has been extensively analyzed in cell cycle checkpoint contexts. Wip1 preferentially targets multiple proteins at their pSQ/pTQ motifs, which are phosphorylated by ATM, ATR, or DNA-PK. In addition, Wip1 also targets pTXpY motifs in p38 mitogen-activated protein kinase (MAPK), which activates p53 upon DNA damage, and in the uracil DNA glycosylase UNG2, which regulates base excision repair (BER; Lu et al., 2004; Takekawa et al., 2000). Wip1 has also been reported to facilitate the reversal of cell cycle checkpoint responses, returning cells to the homeostatic state after completion of DNA repair. Wip1 likely plays a role in the p53 negative feedback loop through two pathways, i.e., dephosphorylation of p38 or p53. Following DNA damage, p53 up-regulates Wip1, which then inhibits p38 via dephosphorylation at T180; inactivated p38 results in inhibition of p53 (Bulavin et al., 1999; Appella and Anderson, 2001). On the other hand, up-regulation of Wip1 reverses p53 activation by dephosphorylating p53 at S15 (Lu et al., 2005). UNG2, another target of Wip1, is phosphorylated and activated in response to UV, inducing BER activity. Wip1 also inhibits BER activity through dephosphorylation of UNG2 at T6 after completion of DNA repair (Lu et al., 2004). Importantly, mice lacking Wip1 are viable but exhibit defects in reproductive organs, immune functions, and cell cycle control (Choi et al., 2002). Knockout of Wip1 triggers p38-mediated activation of the p53, p16, and p19 pathways, leading to enhanced DDRs, promoting genomic stability, and providing resistance to transformation by oncogenes (Bulavin et al., 2004). Consistent with Wip1's function as an oncogene, amplification of this gene has been reported in several human tumors, including breast cancer, neuroblastoma, and ovarian clear cell adenocarcinoma (Bulavin et al., 2002; Li et al., 2002; Hirasawa et al., 2003; Saito-Ohara et al., 2003). In fact, an associated checkpoint phenotype was reported; overexpressed Wip1 cells abrogated S phase and G_2/M DNA damage checkpoints, whereas reduction of Wip1 expression

enhanced the enforcement of intra-S and G_2/M checkpoints (Lu et al., 2005).

PPM1G

PPM1G (also denoted PP2Cγ), a PP2C phosphatase what was originally identified as a splicing factor, has a role in the DDR. PPM1G mediates the exchange of H2A-H2B, which is implicated in the recovery from DNA damage (Kimura et al., 2006). PPM1G-knockdown cells show defects in normal cell proliferation (Allemand et al., 2007), and PPM1G-deficient DT40 cells are sensitive to DNA damage (Kimura et al., 2006), indicating the important role of PPM1G in cell growth and the DDR. Recently, another report demonstrated that PPM1G has a new function in p53 activation through the deubiquitinating enzyme USP7 (also known as HAUSP), which stabilizes the E3 ligase Mdm2 (Khoronenkova et al., 2012). In fact, following IR, ATM phosphorylates and activates PPM1G, which then dephosphorylates and inactivates USP7, leading to Mdm2 degradation and accumulation of p53.

DDR PLAYERS ARE DEPHOSPHORYLATED BY PROTEIN PHOSPHATASES

SENSOR KINASES, ATM, ATR, AND DNA-PK

PP2A

PP2A has been reported to operate as a regulator of ATM (Goodarzi et al., 2004). In the absence of DNA damage, PP2A associates with and dephosphorylates ATM at S1981 (**Figure 1A**). Following DNA damage, rapid dissociation of PP2A from ATM leads to activation of ATM. Inhibition of PP2A by OA or by expressing a dominant-negative mutant of PP2Ac induces autophosphorylation of ATM at S1981 in undamaged cells without activation of ATM activity (Yan et al., 2010). Other reports demonstrated that IR induces dissociation of the B55 subunit from PP2A in an ATM-dependent manner, influencing the disruption of ATM-PP2A (Guo et al., 2002). Despite these studies, the molecular mechanism regulating the dissociation of ATM-PP2A remains to be determined.

Little is known about the role of PP2A in mediating DNA-PK. Studies have shown that the interaction of PP2A with the DNA-PK subunits Ku70 and Ku80 is induced by DSBs. Moreover, PP2A has been shown to dephosphorylate each of these proteins both *in vitro* and *in vivo* (**Figure 1C**). Further functional analyses showed that PP2A-dependent dephosphorylation of DNA-PK subunits enhances the formation of a functional DNA-PK, leading to promotion of NHEJ and DSB repair (Douglas et al., 2001; Wang et al., 2009).

PP1

PP1-dependent DDR regulation is partly mediated by its chromatin targeting subunit, Repo-Man, which was isolated as a PP1γ-specific interacting protein (Trinkle-Mulcahy et al., 2006; Vagnarelli et al., 2006). Studies in *Xenopus* egg extracts demonstrated that Repo-Man interacts with ATM and PP1 through distinct domains, leading to PP1-dependent regulation of ATM phosphorylation and activation (Peng et al., 2010; **Figure 1A**). Following DNA damage, the Repo-Man-PP1γ complex is released from chromatin, leading to activation of ATM at DNA damage sites.

Wip1

Wip1 suppresses ATM activity through dephosphorylation of ATM, resulting in restoration of ATM to its dephosphorylated state after completion of DNA repair (Shreeram et al., 2006; **Figure 1A**). Given the fact that Wip1 is constitutively associated with ATM, how Wip1 activity is regulated remains to be determined.

PP5

Unlike the phosphatases described above, PP5 has a role in the activation of ATM and the association between ATM and PP5 is induced by DNA damage (Ali et al., 2004). Following DSBs, ATM-mediated phosphorylation of Rad17 at pS635 and p53 at S15 is not induced in PP5-knockdown cells, which exhibit an impaired S-phase checkpoint (Ali et al., 2004). In fact, expression of a catalytically inactive PP5 mutant inhibits ATM activation, whereas wild-type PP5 does not affect the phosphorylation status of ATM at S1981 after IR exposure (Ali et al., 2004; Wechsler et al., 2004). These results suggest that PP5 is likely not involved in dephosphorylation of this site, but instead may be involved in the activation of ATM (**Figure 1A**).

Regulatory links between PP5 and ATR as well as PP5 and ATM have been demonstrated (Zhang et al., 2005). PP5 interacts with ATR in a DNA damage-dependent manner, and down-regulation of PP5 leads to defects in the phosphorylation of ATR targets, including Rad17 and Chk1, following UV or HU and an aberrant S-phase checkpoint, indicating the involvement of PP5 in ATR activation (**Figure 1B**). Whether ATR is a substrate of PP5 currently remains unknown.

PP5 interacts with and dephosphorylates DNA-PKcs (Wechsler et al., 2004; **Figure 1C**). Phosphorylation of DNA-PKcs at T2609 and S2056 is reduced in cells overexpressing PP5, suggesting that PP5 mediates dephosphorylation of DNA-PKcs.

PP6

DNA-PKcs associate with PP6 and all regulatory subunits, including PP6R1, PP6R2, and PP6R3, and PP6 is involved in dephosphorylation of DNA-PKcs (Mi et al., 2009b; Douglas et al., 2010; **Figure 1C**). IR enhances this interaction and promotes the import of this complex into the nucleus (Mi et al., 2009b). In contrast, other findings have indicated that the interaction between DNA-PKcs and the PP6 complex is constitutive (Douglas et al., 2010). Although it is not clear whether the interaction between DNA-PKcs and PP6 is indeed induced by DNA damage, Douglas et al. (2010) produced an attractive model in which DNA-PKcs recruit PP6 complexes to damaged sites, permitting PP6 to contribute to the dephosphorylation of H2AX, dissolution of foci, and release from the G_2/M checkpoint.

BAAT1

BRCA1-associated protein required for ATM activation 1 (BAAT1), which was isolated as a BRCA1-interaction partner, is important for activation of ATM (Aglipay et al., 2006; **Figure 1A**). Expression of BAAT1 and association of BAAT1 with ATM are increased after IR. Importantly, phosphorylation of several ATM targets, including H2AX, NBS1 at S343, Chk2 at T68, and ATM

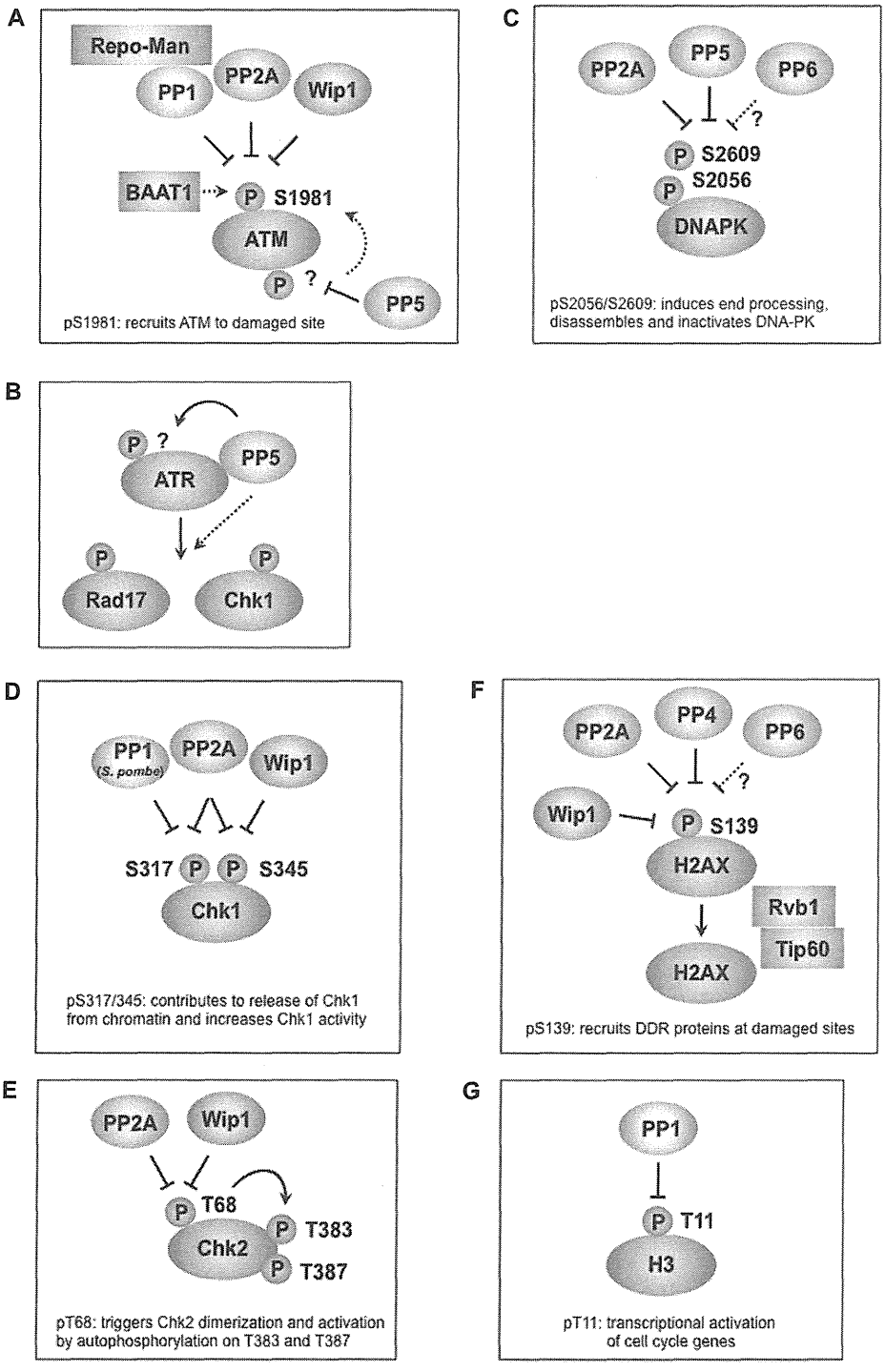

FIGURE 1 | Protein phosphatases regulate multiple phosphorylation events in the DNA damage response. (A) PP1, PP2A, and Wip1 dephosphorylate ATM at S1981, which is required for the recruitment ATM to damage sites. BAAT1 protects ATM from dephosphorylation by phosphatases. PP5 is likely involved in ATM activation through dephosphorylation of ATM, which may induce ATM phosphorylation at S1981. **(B)** PP5 is required for ATR- targeted phosphorylation of Rad17 and Chk1. Although PP5 associates with ATR in a DNA damage-dependent manner, the precise mechanism remains to be determined. **(C)** PP2A, PP5, and possibly PP6 dephosphorylate multiple sites on DNA-PK, including S2056 and S2609. These sites are autophosphorylated by DNA-PK and are involved in the activation/inactivation of DNA-PK. **(D)** PP1 (*S. pombe*), PP2A, and Wip1 dephosphorylate Chk1 at S317 and/or S345, which promotes its release from chromatin and increases Chk1 kinase activity. **(E)** PP2A and Wip1 mediate the dephosphorylation of Chk2 at T68, which facilitates Chk2 dimerization and

(Continued)

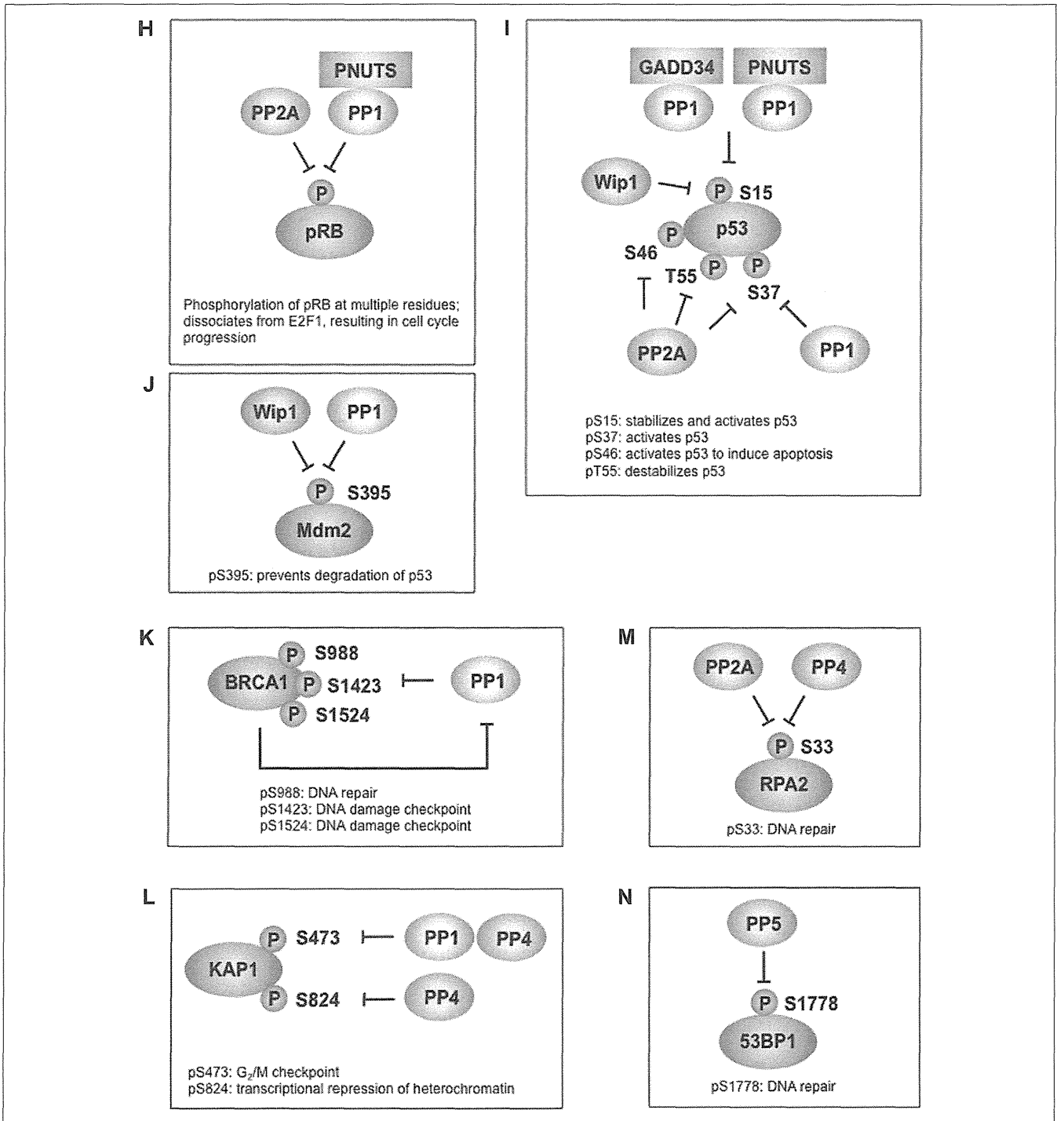

FIGURE 1 | autophosphorylation at T383 and T387. **(F)** γ-H2AX (the phosphorylated form of H2AX at S139) is required for recruitment of various DDR proteins to damaged sites and is dephosphorylated by PP2A, PP4, PP6, and Wip1. Rvb1/Tip60 is implicated in the removal of γ-H2AX. **(G)** PP1 dephosphorylates H3 at T11 following DNA damage, leading to transcriptional repression of cell cycle-regulated genes. **(H)** PP2A and PP1-PNUTS dephosphorylate pRb at multiple sites, leading to inhibition of E2F1 activity and cell cycle arrest. **(I)** p53 is dephosphorylated at S15 by PP1-GADD34, PP1-PNUTS, and Wip1, resulting in p53 inactivation. S37 dephosphorylation is also mediated by PP1 and PP2A. PP2A also dephosphorylates p53 at S46 and T55. **(J)** Wip1 and PP1 dephosphorylate Mdm2 at S395, which facilitates p53 degradation. **(K)** PP1 interacts with BRCA1 and dephosphorylates multiple sites of BRCA1. In addition to acting as a PP1 substrate, BRCA1 also plays a role in PP1 inhibition. **(L)** KAP-1 is dephosphorylated at S473 by PP1 and PP4, whereas S824 is dephosphorylated by PP4. **(M)** PP2A and PP4 are required for RPA2 dephosphorylation. **(N)** Phosphorylated 53BP1 is recruited to DNA damage sites to coordinate the localization of DDR factors and promote their activation. PP5 dephosphorylates 53BP1 at S1778, leading to 53BP1 release from DNA damage sites.

at S1981, is not induced in BAAT1-knockdown cells. Defects in ATM phosphorylation at S1981 observed in BAAT1-knockdown cells could be restored by OA treatment.

TRANSDUCER KINASES, Chk1/Chk2

PP2A

During the normal unperturbed cell cycle, Chk1 is phosphorylated on S317 and S345 by ATR, and in turn, phosphorylated Chk1 is antagonized by Chk1-regulated PP2A to maintain the status of Chk1 activity (**Figure 1D**). Thus, the activity of Chk1 is finely tuned in an ATR-Chk1-PP2A regulatory loop (Leung-Pineda et al., 2006).

PP2A was also reported to interact with Chk2 and regulates phosphorylation at T68 of Chk2 after DNA damage (Dozier et al., 2004; Liang et al., 2006; Freeman et al., 2010; **Figure 1E**). Studies have suggested that PP2A maintains Chk2 in an inactive state under normal conditions, while PP2A dissociates from Chk2 and permits the phosphorylation of Chk2 by ATM under DNA damage conditions. After completion of DNA repair, PP2A has a role in attenuating the DDR partly through dephosphorylation of Chk2.

Wip1

Wip1 binds Chk1 and dephosphorylates S345 and, to a lesser extent, S317, leading to inhibition of Chk1 activity (Lu et al., 2005; **Figure 1D**). Thus, Wip1 has a role in abrogating cell cycle checkpoints, in part through dephosphorylation of Chk1.

Wip1 also interacts with Chk2 and dephosphorylates Chk2 at T68 (Fujimoto et al., 2006; Oliva-Trastoy et al., 2007; **Figure 1E**). Knockdown of Wip1 leads to sustained phosphorylation of Chk2 at T68, promoting apoptosis in response to DNA damage. Consistent with this observation, overexpression of Wip1 antagonizes Chk2 activation. Thus, Wip1 is thought to play a negative role in DNA damage-induced apoptosis by dephosphorylation and inactivation of Chk2.

PP5

Upon UV irradiation, ATR-mediated phosphorylation of Chk1 at S345 is increased and maintained in PP5-depleted cells. After 24-h exposure to UV irradiation, this site is dephosphorylated to control levels, indicating that PP5 is not the only phosphatase mediating Chk1 at S345 (Amable et al., 2011). Importantly, PP5-knockout MEFs also exhibit prolonged and enhanced phosphorylation of Rad17, H2AX, and Chk1 at S317. However, contrary to this observation, one study has shown that knockdown of PP5 by antisense PP5 or ectopic expression of a catalytically inactive PP5 mutant leads to impairment of the ATR-mediated phosphorylation of Rad17 and Chk1 (Zhang et al., 2005). The precise functions of PP5 in the DDR remain to be determined.

PP1

The involvement of PP1 in checkpoint recovery is less well studied. However, a study in *Schizosaccharomyces pombe* demonstrated that dephosphorylation of Chk1 by the PP1 homolog Dis2 allows mitotic entry upon completion of DNA repair in G_2 phase (den Elzen and O'Connell, 2004; **Figure 1D**). However, in human cells, knockdown of PP1 does not change the phosphorylation status of Chk1 on S317, and PP1 does not dephosphorylate Chk1 directly (Leung-Pineda et al., 2006).

HISTONES AND HISTONE VARIANTS

H2AX-pS139 (γ-H2AX)

PP4 PP4 dephosphorylates γ-H2AX *in vitro*, and knockdown of PP4 shows persistent γ-H2AX without apparent deficiencies in DNA repair following IR, suggesting that PP4 has a direct role in the dephosphorylation of γ-H2AX (Nakada et al., 2008; **Figure 1F**). Indeed, PP4C knockdowned cells display a prolonged G2/M checkpoint arrest after IR. It is also reported that PP4 is required to repair DNA replication-mediated DNA damage and PP4 silenced cells are sensitive to DNA replication inhibitors (Chowdhury et al., 2008).

PP2A In response to DNA damage, PP2A forms foci and colocalizes with γ-H2AX and dephosphorylates γ-H2AX (Chowdhury et al., 2005; **Figure 1F**). However, since repair of damaged DNA is delayed in PP2A-depleted cells, the PP2A-dependent increase in γ-H2AX may be partly due to reduced repair (Chowdhury et al., 2005; Nakada et al., 2008).

PP6 Down-regulation of either PP6C or PP6R1 causes extensive γ-H2AX and persistent γ-H2AX foci formation following DNA damage, suggesting that PP6 plays a role in the dephosphorylation of γ-H2AX (Douglas et al., 2010; **Figure 1F**). It is important to note that knockdown of PP6 did not affect the phosphorylation of ATM at S1981, SMC1 at S957, or Chk2 at T68 (Douglas et al., 2010). In the context of cisplatin-induced DSBs, PP6 is required for homologous recombination; thus, persistent γ-H2AX in PP6-depleted cells can be explained by delayed DSB repair (Zhong et al., 2011).

Wip1 A recent study reported that Wip1 binds directly to H2AX and dephosphorylates it *in vitro* and *in vivo*, leading to reverse checkpoint signaling (Cha et al., 2010; **Figure 1F**). Moreover, ectopic expression of Wip1 reduces IR-induced γ-H2AX and foci formation for several DDR factors, leading to delayed DNA repair after IR. However, whether knockdown of Wip1 affects DNA repair efficiency remains unknown.

Histone H3

PP1 We have recently identified a novel function for Chk1 as a transcriptional regulator through phosphorylation of H3 at T11 (H3-pT11; Shimada and Nakanishi, 2008; Shimada et al., 2008). This phosphorylation appears to activate the GCN5 histone acetyltransferase complex, leading to H3K9 acetylation and transcription of critical cell cycle regulatory genes, such as *cdk1* and *cyclin B1*. Upon DNA damage, Chk1 rapidly dissociates from chromatin, H3T11 phosphorylation and H3K9 acetylation levels are reduced, and target genes are repressed. In addition to release of Chk1 from chromatin, we recently reported that activation of protein phosphatase 1 is involved in the reduction of H3-pT11 following DNA damage through suppression of T311 phosphorylation due to decreased Cdk1 activity (Shimada et al., 2010; **Figure 1G**).

THE EFFECTOR MOLECULES pRb, p53, AND Mdm2

PP1

Retinoblastoma tumor suppressor protein (pRb), which is negatively regulate cell cycle progression, can interact with all PP1

isoforms (Durfee et al., 1993; Vietri et al., 2006), and PP1 dephosphorylates and activates pRb at the mitosis-to-interphase transition (Alberts et al., 1993; Durfee et al., 1993; Ludlow et al., 1993; Nelson et al., 1997; **Figure 1H**). Importantly, recent data revealed that PP1 competes with Cdks for binding to pRb (Hirschi et al., 2010). PP1 regulatory factors have also been implicated in the regulation of pRb. One of the regulatory subunits, PNUTS dissociates from PP1 under hypoxia stress, leading to activation of PP1, dephosphorylation of pRb at T821, and inhibition of cell growth (Udho et al., 2002; Krucher et al., 2006). Importantly, depletion of PNUTS in cancer cells, but not in normal cells, induces apoptosis through the activation of PP1 and its subsequent regulation of pRb (Krucher et al., 2006; De Leon et al., 2008).

p53 is phosphorylated on pS15 upon DNA damage by ATM/ATR and contributes to stabilization and activation of p53 (Dumaz and Meek, 1999; Lu et al., 2005). Phosphorylation of p53 at S37, which is also transiently up-regulated upon DNA damage, is required for p53 transcriptional activity (Dohoney et al., 2004). PP1 dephosphorylates p53 at S15 and S37 *in vitro* and *in vivo*, reducing transcriptional activity and attenuating apoptosis (Li et al., 1998, 2006; **Figure 1I**). Growth arrest and DNA damage 34 (GADD34) is known to inhibit the binding of PP1 to p53 and prevent dephosphorylation of p53 at S15 (Li et al., 1998). In addition to GADD34, PNUTS also inhibits PP1-dependent dephosphorylation of p53 at S15 and plays a role in apoptosis via regulation of p53 (Lee et al., 2007b). Thus, the association of regulators such as GADD34 and PNUTS with PP1 is required PP1-mediated regulatory activity.

p53 is also regulated indirectly through Mdm2. DNA damage-induced phosphorylation of Mdm2 at S395 by ATM attenuates the ability of Mdm2 to promote nuclear export and degrade p53 (Maya et al., 2001). Once p53 is stabilized and activated, PP1 triggers the inactivation of the signaling cascade (**Figure 1J**). Dephosphorylation of Mdm2 inhibits it autoubiquitination, resulting in stabilization, which triggers degradation of p53 (Lu et al., 2007).

PP2A

PP2AC physically associates with pRb, p107, and p130 *in vivo* (Cicchillitti et al., 2003; Garriga et al., 2004) and mediates oxidative stress-induced dephosphorylation of these proteins (Cicchillitti et al., 2003; Magenta et al., 2008). pRb can also be dephosphorylated by PP2A after IR, which may trigger the recruitment of pRb to replication initiation sites, thereby suppressing abnormal replication (Avni et al., 2003; **Figure 1H**).

PP2A binds to p53 following IR and dephosphorylates multiple sites, S37, S46, and T55 to control p53 activity (Dohoney et al., 2004; Li et al., 2004; Mi et al., 2009a; **Figure 1I**). Under normal cell growth conditions, p53 is phosphorylated at T55 by TATA box binding protein-associated factor 1 (TAF1), resulting in Mdm2-mediated p53 degradation (Li et al., 2004). In response to DNA damage, two reactions trigger dephosphorylation of p53 at T55 and stabilization of p53. One is mediated by the dissociation of TAF1 from p53, while the other occurs through dephosphorylation of B56γ-containing PP2A complexes (Li et al., 2007). B56γ and PP2AC levels are increased upon DNA damage, contributing to PP2A-mediated dephosphorylation of p53 at T55 (Dohoney et al., 2004; Li et al., 2007).

Wip1

Wip1 can dephosphorylate p53 on S15 *in vitro* (Lu et al., 2005; **Figure 1I**). In addition, ectopic expression of Wip1 decreases p53 protein levels and S15 phosphorylation, whereas knockdown of Wip1 results in increased p53 protein levels and S15 phosphorylation. Thus, Wip1 mediates dephosphorylation of p53 at S15.

Wip1 is also known to target Mdm2 at S395, promoting the stability of Mdm2 and enhancing the interaction between Mdm2 and p53 (Maya et al., 2001; Lu et al., 2007; Yamaguchi et al., 2007; **Figure 1J**).

OTHERS

BRCA1

The breast cancer susceptibility gene BRCA1 plays multiple roles in the DDR, such as DNA repair and S and G_2/M checkpoint control (Huen et al., 2010). BRCA1 has a RING finger domain and two BRCA1 terminal domains (so-called BRCT domains) involved in associations with other proteins. DNA damage induces the phosphorylation of BRCA1 at multiple residues, such as S1524 and S1423 by ATM and ATR, respectively (Cortez et al., 1999; Tibbetts et al., 2000), and S988 by Chk2 (Lee et al., 2000). BRCA1 is rapidly localized to damage sites, which contain DNA repair proteins such as Rad51. The PP1α catalytic subunit interacts with BRCA1 and dephosphorylates the sites phosphorylated by ATM, ATR, and Chk2 (Liu et al., 2002; Hsu, 2007; **Figure 1K**). Mutational research of the PP1-binding motif in BRCA1 has revealed that the interaction between BRCA1 and PP1α is important for proper relocation of BRCA1 and Rad51 to DNA damage sites and consequently is important for the DNA repair function of BRCA1. In addition, BRCA1 inhibits PP1α activity, although the precise mechanism underlying this regulatory event remains to be determined (Liu et al., 2002).

KAP1

Phosphorylation of KAP-1 by ATM has been implicated in chromatin relaxation at sites of DSBs (Ziv et al., 2006; Goodarzi et al., 2008), a process that is necessary to permit the recruitment of DDR factors to the damaged DNA. Lee et al. (2010) extensively studied KAP-1 as a PP4 substrate and found that PP4 controls 2IR-mediated phosphorylation sites on KAP-1, i.e., ATM-dependent phosphorylation at S824, which is important for transcriptional repression of heterochromatin, and Chk2-dependent phosphorylation at S473, which is involved in the G_2/M DNA damage checkpoint (Lee et al., 2010; **Figure 1L**). Moreover, a recent study also revealed that PP1 mediates dephosphorylation of KAP1 at S473 and sumoylation of KAP-1 to counter the effect of ATM (Li et al., 2010; **Figure 1L**).

RPA2

RPA is a trimeric protein complex involved in DNA replication, DNA repair, and recombination. ATM, ATR, and DNA-PK phosphorylate one of the subunits, RPA2, and this phosphorylation event is important for the DNA repair function of the enzyme (Wang et al., 2001; Sakasai et al., 2006; Anantha et al., 2007). In addition to phosphorylation, timely dephosphorylation of RPA2 is required for the recruitment of the homologous recombination